

pubs.acs.org/Macromolecules Article

Bridging Field Theory and Ion Pairing in the Modeling of Polyelectrolytes and Complex Coacervation

Charles E. Sing* and Jian Qin



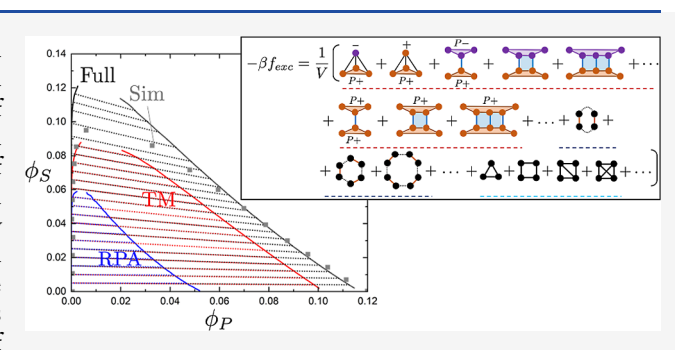
Cite This: *Macromolecules* 2023, 56, 5941–5963



ACCESS I

III Metrics & More

ABSTRACT: Complex coacervation is a phase separation phenomenon driven by the electrostatic attraction between oppositely charged macromolecular species. A recent surge of interest in coacervation between polyelectrolytes has been driven by both fundamental advances in experimental characterization of these systems and recognition of their relevance for both biological systems such as biomolecular condensates as well as industrially relevant consumer products. Concomitantly, there have been several theories capable of predicting complex coacervation that are used to explain these experimental observations. While there has been a general conceptual consensus on the underlying physics of



Article Recommendations

coacervation, these theoretical approaches have so far remained distinct. Polymer field theory, liquid state theory, ion pairing theories, and scaling theories all provide useful insights, but how the assumptions of each candidate theory are interrelated remains largely unexplored. In this paper, we attempt to show how two such classes of models can be derived from a single starting point using cluster expansions as the basis for discussing which interactions are included in both field theory and ion pairing theory. This allows us to compare and contrast these approaches, evaluate conditions where each model should be relevant, and suggest ways in which existing models can be improved or parameterized.

INTRODUCTION

Oppositely charged macromolecules can undergo an associate phase separation in a process known as complex coacervation. 1-3 In this process, any combination of macromolecular species, including colloidal particles, 4 proteins, 5-7 surfactants, 8 and polymers, can form a dense "coacervate" phase that maximizes favorable electrostatic interactions and a dilute "supernatant" phase that is composed mostly of solvent and small-molecule salt ions.² This macroscopic phase separation was first identified in 1929 by Bungenberg de Jong and Kruyt,10 and since then, there has been sustained progress in our understanding of these materials. This has been spurred in large part by their relevance to food science and personal care products 11-13 in which coacervates are used as viscosity modifiers and encapsulants and can be made using biopolymers. Recently, however, there has been a surge of interest in coacervation¹ driven by their promise as a biomaterial for protein encapsulation^{14–17} and as an analogue to help understand liquid-liquid phase separation phenomena in cells. 18-22 This has led to a large number of fundamental experimental studies²³⁻³⁵ probing the thermodynamics and structure of coacervates, with a particular focus on coacervates formed between oppositely charged polyelectrolytes. These experiments have established some of the first comprehensive phase diagrams mapping out a rather large parameter space, 23,28,30,36-38 seeking to understand the role of chain length, ^{23,28,30} salt concentration, polymer concentration, polarity, ³⁶ stoichiometry, ³⁹ chain flexibility, ⁴⁰ valency, ²⁹ temperature, ⁴¹ monomer sequence, ^{42,43} crowding, ⁴⁴ and pH. ^{35,37,45} A systematic study of this wide variety of parameters has facilitated the use of coacervates in self-assembly, ^{46–55} drug delivery, ^{17,56} and other materials applications. ^{57–64} A wide range of characterization methods have been used in pursuit of understanding phase behavior, including turbidity measurements, ^{29,34} thermogravimetric analysis, ^{28,37,38} and fluorescence. ^{23,36} This has been coupled with isothermal titration calorimetry ^{34,42} to understand coacervation thermodynamics and scattering to understand polymer structure. ^{27,53}

Concomitant with experimental efforts to understand complex coacervates, theory and simulation have been used to provide molecular interpretation and insight into the physical origins of phase separation. The earliest example, which remains a commonly used model for coacervation, is the Voorn–Overbeek model. This original model combined the

Received: May 23, 2023 **Revised:** July 11, 2023 **Published:** July 26, 2023





Flory—Huggins theory of polymer solutions⁶⁸ with the Debye—Hückel theory of dilute electrolytes⁶⁹ to establish a free energy expression that can predict coacervation. We will discuss this model in more detail later, but it informed a lot of early work on coacervation;^{23,66,67} phase separation is observed at low salt and polymer concentrations wherein electrostatic interactions are weakly screened, while the system is miscible at high salt and polymer concentrations. Unphysical choices of model parameters lead to superficial agreement between Voorn—Overbeek and some aspects of coacervate phase diagrams.²³ This model has also been used in predictions for interfacial tension,⁷⁰ ion partitioning,⁷⁰ and as a way to explain time-salt superposition in rheological measurements.²⁶

It is now accepted that Voorn-Overbeek neglects several important physical features.³⁰ This is unsurprising as the Debye-Hückel model does not account for the connected nature of the polyelectrolytes, is limited to dilute electrolyte concentrations,⁷¹ and neglects the finite volume of the polymer and salt species.^{30,72} This means that the parameters used to match Voorn-Overbeek to experimental phase diagrams generally lack physical meaning. Subsequent theoretical modeling has sought to develop a more sophisticated physical picture of coacervation, with most theories addressing some or all of these issues. In this effort, there has been a proliferation of possible coacervate models, building on the various theoretical approaches common in the field of polymer physics. Most connected to Voorn-Overbeek, polymer field theory has been widely used to include the effects of connectivity and the effects of fluctuating charge. 73-83 Simplified representations of the excluded volume are considered in several of these models, 75,76 though typically relying on (for example) Gaussian-smeared distributions of charged species. ^{21,79–86} Relatedly, scaling theory is also used to capture key length scales associated with electrostatic interactions and polymer conformations, 87-94 including connectivity but requiring ad hoc modifications to describe highly correlated electrolytes. 95 Liquid state theory is a traditional way to addressing these strong correlations in charged systems and has been used to predict coacervate phase behavior; 72,96,97 however, the use of complicated closure relationships limits the practical application of these models beyond simple homopolyelectrolyte coacervates. Finally, ion pairing theory is a broad class of models that uses simplified arguments to account for these same correlations, $^{36,43,98-109}_{}$ but it has to this point been largely accounted for in an ad hoc fashion. This includes both "effective" ion pairing or binding reactions $^{36,99-101,109}$ and the transfer matrix (TM) model developed by the authors.

Taken as a whole, these theoretical approaches all provide a coherent picture of coacervation, though each method has its own limits of applicability. A key variable in this regard is the linear charge density, ^{30,43,72,85,95,110,111} which affects the strength of charge correlations (e.g., such as those related to counterion condensation), ^{72,112,113} indirectly sets the overall density of charged species, ^{30,43} and governs the putative mechanism of coacervation. ¹¹⁰ Generally speaking, polymer field theory and scaling theory exhibit fluctuation-driven coacervation, where attractions are governed by Gaussian chain statistics between widely spaced charged monomers. ¹ Conversely, liquid state and ion pairing theories rely on interactions governed by strong correlations between tightly connected charged monomers. ¹ Evidence in both experiments and simulations support this distinction ^{43,95,111,114} and has prompted efforts to either include correlations into field/scaling

theories 92,95 or to include fluctuating chain statistics into ion pairing theories. 100,109 Despite progress, however, the formal differences between these various approaches frustrates attempts at comparison or consolidation. This is exacerbated by another major factor; experiment is not always discerning, as most coacervate theories at least provide plausible phase diagrams and correct trends, 23,28,30,36,37,70,108,111 with differences easily (and often correctly) attributed to the specific chemistries used in a given experiment. This means that most theoretical approaches have some successful experimental comparison to support their method. This is positive in that theorists in the field are working in close concert with experimental collaborators, but they can muddle the advantages and disadvantages of the various approaches. There is thus a need to establish a shared theoretical basis that can clarify the approximations inherent to each approach.

In this paper, we show that a cluster expansion approach provides a common starting approach for several key classes of coacervate theory currently in the literature. We build off the standard approaches taken by Mayer to derive Debye-Hückel theory using cluster expansions 115 and thus re-derive Voorn-Overbeek; 66,67 however, we show that variations of this approach can be used to justify several other models spanning polymer field theory and ion pairing theories. We show how different choices of approximation, presented in the context of cluster expansions, give rise to the different models and particularly why linear charge density is such an important variable for model selection. We can then develop a metric to quantify the boundary between high charge-density and low charge-density approaches. Finally, we propose a modified version of the TM theory, which combines several of the new insights gained by considering what is accounted for in other models.

CLUSTER EXPANSION AS A COMMON STARTING POINT

The coacervation models we discuss can all be derived from the expression for the grand canonical partition function of a system with n_{P+} polycation chains, n_{P-} polyanion chains, n_{+} cations, and n_{-} anions

$$\Xi = \sum_{n_{p_{+}}}^{\infty} \sum_{n_{p_{-}}}^{\infty} \sum_{n_{+}}^{\infty} \sum_{n_{-}}^{\infty} \frac{1}{n_{p_{+}}! n_{p_{-}}! n_{+}! n_{-}!} \int \mathcal{D}\mathbf{r}_{p_{+}}^{n_{p_{+}}} P_{p_{+}}(\{\mathbf{r}_{p_{+}}^{n_{p_{+}}}\})$$

$$\int \mathcal{D}\mathbf{r}_{p_{-}}^{n_{p_{-}}} P_{p_{-}}(\{\mathbf{r}_{p_{-}}^{n_{p_{-}}}\}) \times \int d\mathbf{r}_{+}^{n_{+}} \int d\mathbf{r}_{-}^{n_{-}} \prod_{\alpha} \prod_{i=1}^{n_{\alpha}N_{\alpha}} z_{\alpha}^{*}(i)$$

$$\prod_{\gamma} \prod_{j}^{n_{\gamma}N_{\gamma}} e_{\alpha,\gamma}(i,j)$$
(1)

We are using a shorthand here to simplify this expression. The products over α and γ are over the species (P+, P-, +, and -) that interact via electrostatics. The product over indices i and j represents products over all particles (or monomers) in each species, of which there are $n_{\alpha}N_{\alpha}$ particles for each. N_{α} is the degree of polymerization of α , with $N_{\alpha=\pm}=1$ for non-polymeric species. There are integrals over the positions of salt or monomer particles, with the path integral denoting the integration over all monomer positions for a given chain. The intra-chain structure is imposed by the weighting factor $P_{p-}(\{\mathbf{r}_{p-}^{n_{p+}}\})$ that can account for chain connectivity, flexibility, and so forth. The intra-this notation, we start by assuming that

all monomers are disconnected ($P_{P\pm}=1$), justifying the integral over (for example) $n_{P+}N_{P+}$ individual particles. The quantity $z_{\alpha}^*(i) = \exp[\beta(\mu_{\alpha} - \phi_{\alpha}(\mathbf{r}_i))]$ is the activity of the i-th particle of species α in a spatially varying field $\phi_{\alpha}(\mathbf{r})$ and with a chemical potential μ_{α} with the asterisk distinguishing between activity and charge valency. The Boltzmann factor associated with the pair potential between a pair of particles i and j of species α and γ is given as $e_{\alpha,\gamma}(i,j) = \exp[-\beta u_{\alpha,\gamma}(\mathbf{r}_i v_j)]$. In this implicit solvent formalism, the pairwise interaction $u_{\alpha,\gamma}(\mathbf{r}_i v_j)$ is the potential of mean force between particles of type α and γ due to the classical McMillan—Mayer theory. ¹¹⁸

It is possible to write this partition function in a more concise way via the well-known "cluster expansion" 119

$$\Xi = 1 + \bullet + \bullet - \bullet + \triangle + \square + \cdots$$

Here, the circles are "z-circles" that indicate a contribution from factors $z_{\alpha}^*(i)$ for each circle in the diagram, and the connecting gray lines are "e-bonds" that represent the Boltzmann factors $e_{\alpha,\gamma}(i,j)$ for each pair of particles. Note that in this four-component model, each circle implies a summation over all possible species α , which in this case includes all of the charged (i.e., non-water) particles. Therefore, we also consider all combinations of $e_{\alpha,\gamma}(i,j)$ between each pair of factors $z_{\alpha}^*(i)$ and $z_{\gamma}^*(j)$. For example, the fourth (i.e., three z-circle) term in this expansion can be written as

[fourth diagram] =
$$\frac{1}{6} \sum_{\alpha,\gamma,\zeta} \int d\mathbf{r}_i d\mathbf{r}_j d\mathbf{r}_k z_{\alpha}^*(i) z_{\gamma}^*(j) z_{\zeta}^*(k)$$
$$e_{\alpha,\gamma}(i,j) e_{\gamma,\zeta}(j,k) e_{\alpha,\zeta}(i,k) \tag{2}$$

Standard diagrammatic techniques lead to the classical result that the excess Helmholtz free energy density $\beta f_{\rm exc} = \beta f - \beta f_{\rm id}$ beyond the ideal contribution $f_{\rm id}$ can be written in the diagrammatic form ¹¹⁹

$$-\beta f_{exc} = \frac{1}{V} \left[\bullet \bullet + A + \Box + \Box + \Box + \Box + \Box + \cdots \right]$$

This set includes all irreducible diagrams (see definition in Section 3.7 of ref 119)¹¹⁹ consisting of at least two circles and now uses ρ -circles that contribute factors $\rho_{\alpha}(i)$ and black "fbonds", which are related to e-bonds by $e_{\alpha\gamma}(i,j) = f_{\alpha\gamma}(i,j) + 1.$ 71,119 We note that the summation over species index α is implied by each ρ_{α} -circle and that at most, one f-bond is permitted between two ρ -circles. As an example, the second term on the right side is given as

$$\begin{split} & \frac{[\text{second diagram}]}{V} = \frac{1}{6V} \sum_{\alpha,\gamma,\zeta} \int \mathrm{d}\mathbf{r}_i \mathrm{d}\mathbf{r}_j \mathrm{d}\mathbf{r}_k \rho_\alpha(i) \rho_\gamma(j) \rho_\zeta(k) \\ & f_{\alpha,\gamma}(i,j) f_{\gamma,\zeta}(j,k) f_{\alpha,\zeta}(i,k) = \frac{1}{6V} \sum_{\alpha,\gamma,\zeta} \rho_\alpha \rho_\gamma \rho_\zeta \int \mathrm{d}\mathbf{r}_i \mathrm{d}\mathbf{r}_j \mathrm{d}\mathbf{r}_k \\ & f_{\alpha,\gamma}(i,j) f_{\gamma,\zeta}(j,k) f_{\alpha,\zeta}(i,k) \end{split}$$

Here, 1/6 is a combinatoric factor that is determined from the symmetry of an unlabeled diagram, accounting for the number of ways in which the diagram can be rearranged yet retain the same topology. In the second version of the above expression, we use the assumption that we will make in the rest of this paper, in that we will assume a homogeneous phase where the density $\rho_{\alpha}(\mathbf{r}) = \langle \rho_{\alpha} \rangle = \rho_{\alpha}$ is given by its average value. This diagrammatic representation of the excess free energy density will be the starting point of most coacervate models as it isolates the theoretically challenging aspect of the model. The ideal mixing

entropy common to essentially all coacervation models is given

$$\beta f_{id} \nu_0 = \frac{\phi_{P+}}{N_{P+}} \ln \phi_{P+} + \frac{\phi_{P-}}{N_{P-}} \ln \phi_{P-} + \phi_+ \ln \phi_+ + \phi_- \ln \phi_- + \phi_W \ln \phi_W$$
(4)

Consistent with our previous notation, this equation constitutes the Flory–Huggins entropy of mixing of all the species, ⁶⁸ including the polycation (P+), polyanion (P-), cation (+), anion (–), and water solvent (W), with the parenthesis indicating the corresponding subscript. The values ϕ_{α} and N_{α} are the volume fraction and molecular weight, respectively, of component α , assuming a reference volume ν_0 that is the molar volume of the salt, monomer, and water species.

In this paper, we will consider a variety of different approximations of the cluster expansion of the excess free energy, which will be added on to the ideal free energy expression given in eq 4. The total free energy density $\beta f \nu_0 = \beta f_{\rm id} \nu_0 + \beta f_{\rm exc} \nu_0$ can then be compared against previous models in the literature, such that we can establish relationships between these models via their inclusion or neglect of various terms in the cluster expansion.

VOORN-OVERBEEK THEORY

The Voorn–Overbeek model is a simple combination of the results of two classical theories, Flory–Huggins ⁶⁸ and Debye–Hückel, ⁶⁹ to yield a free energy density $\beta f_{\rm VO} \nu_0^{66,67}$

$$\beta f_{\text{VO}} \nu_0 = \frac{\phi_{p_+}}{N_{p_+}} \ln \phi_{p_+} + \frac{\phi_{p_-}}{N_{p_-}} \ln \phi_{p_-} + \phi_+ \ln \phi_+ + \phi_- \ln \phi_-$$

$$+ \phi_{\text{W}} \ln \phi_{\text{W}} - \frac{\kappa^3 \nu_0}{12\pi}$$
(5)

The final term is the excess free energy contribution, which comes from Debye–Hückel theory. The quantity $\kappa = (4\pi\lambda_{\rm B}\sum_{\alpha}\rho_{\alpha}z_{\alpha}^2)^{1/2} \text{ is the inverse Debye screening length of an electrolyte with species }\alpha \text{ with number concentration }\rho_{\alpha} \text{ and valency }z_{\alpha}^{-71}\lambda_{\rm B} = e^2/(4\pi\epsilon_0\epsilon_{\rm r}k_{\rm B}T) \text{ is the Bjerrum length,}^{-71} \text{ where }e \text{ is the elementary charge, }\epsilon_0 \text{ is the permittivity of free space, }\epsilon_{\rm r} \text{ is the relative dielectric constant, and }T \text{ is the temperature. The classical derivation of Debye–Hückel theory is found in most statistical mechanics textbooks,}^{-71}\text{ but yet it is instructive to demonstrate how this expression emerges from the cluster expansion approach that was originally used by Mayer.}^{-115}$

Mayer's approach considered the Coulomb interaction $\beta u_{c,\alpha,\gamma} = \lambda_B z_\alpha z_\gamma / |\mathbf{r}_{i,\alpha} - \mathbf{r}_{j,\gamma}|$ and derived a series of so-called "ring" diagrams that are the dominant and non-zero terms in the excess free energy expansion ^{69,115}

In this approach, the connecting lines are now Ψ -bonds such that $\Psi_{\alpha,\gamma}(\mathbf{r}_i,\mathbf{r}_j) = -\beta u_{c,\alpha,\gamma}(\mathbf{r}_i,\mathbf{r}_j)$. The circles are still ρ -circles. These diagrams are typically evaluated in **k**-space, with each Ψ -bond between species α and β contributing a factor of $4\pi\lambda_{\rm B}z_{\alpha}z_{\beta}\psi(k)$ (with the Fourier transform of the 1/r potential being $4\pi\psi(k) = 4\pi/k^2$) and each ρ -circle contributing a ρ_{α} . Correctly accounting for combinatoric factors associated with the rings, $7^{1,119}$ we can evaluate this diagrammatic expression to yield the Debye–Hückel result

$$\beta f_{\text{exc}} = \frac{1}{2(2\pi)^3} \int d\mathbf{k} \left[-\frac{(\kappa^2 \psi(k))^2}{2} + \frac{(\kappa^2 \psi(k))^3}{3} - \frac{(\kappa^2 \psi(k))^4}{4} + \cdots \right] = \frac{1}{2(2\pi)^3}$$

$$\int d\mathbf{k} [-\kappa^2 \psi(k) + \ln[1 + \kappa^2 \psi(k)]] = -\frac{\kappa^3}{12\pi}$$
 (6)

Including the reference volume ν_0 of the monomer/salt/solvent species, we can thus write the Voorn–Overbeek expression as follows 66,67

$$\beta f_{VO} \nu_0 = \beta f_{id} \nu_0 + \beta f_{exc} \nu_0$$

$$= \frac{\phi_{p_+}}{N_{p_+}} \ln \phi_{p_+} + \frac{\phi_{p_-}}{N_{p_-}} \ln \phi_{p_-} + \phi_+ \ln \phi_+ + \phi_- \ln \phi_-$$

$$+ \phi_W \ln \phi_W - \frac{\nu_0 \kappa^3}{12\pi}$$
(7)

A more complete derivation of both the ring diagrams and their evaluation for a coacervate system are given in Appendix A. This classical derivation is a long-established result in statistical mechanics. However, we will find that this version of the derivation (i.e., using the cluster expansion) was useful to (1) establish its connection to other theories and (2) to illustrate how we will be using the diagrammatic representation of the excess free energy.

■ RPA FROM A CLUSTER EXPANSION APPROACH

The primary way to account for connectivity in polymer melts and solutions, beyond mean-field models such as the Flory—Huggins theory, ⁶⁸ is to use the random phase approximation (RPA) that accounts for harmonic fluctuations in the density fields. Indeed, a large amount of work has used the RPA to study coacervate or polyelectrolyte complex phase behavior, ^{73–77} with several modifications to account for excluded volume and non-Gaussian conformations. ^{75–77} We can show that this cluster expansion approach is capable of reproducing the fundamental result, given by Kudlay and Olvera de la Cruz^{75,76} and later generalized by Qin and de Pablo. ⁷⁷

$$\beta f_{\text{exc}} \nu_0 = \frac{\nu_0}{4\pi^2} \int_0^\infty dk k^2 \ln \left[1 + \frac{\kappa^2 N}{k^2} g_{\text{D}}(k^2 R_{\text{g}}^2) \right]$$
 (8)

To derive this using the cluster expansion approach, we must re-define what we mean by $z_{\alpha}^*(i)$ and $e_{\alpha,\gamma}(i,j)$ (or similarly $f_{\alpha,\gamma}(i,j)$ j)); instead of considering all of the monomers as independent particles, we now use the reference interaction site model (RISM) formalism that treats the monomers as "sites" on polymers that are instead considered the particle units. 120 This requires essentially no change to eq 1, except for several redefinitions; first, the products over particles go to, for example, n_{α} rather than $n_{\alpha}N_{\alpha}$, because the entire polymer chain (and not the monomer) is represented by a single "particle". Second, the quantity $z_{\alpha}^{*}(i) = \exp[\beta(\mu_{\alpha} - \sum_{s=1}^{N_{\alpha}} \varphi_{\alpha}(\mathbf{r}(s)))]$ for polymeric species now sums over the Boltzmann factors of each monomer of species α in the external field ϕ_{α} . Finally, the quantity $f_{\alpha,\gamma}(1,2)$ is now dependent on contributions of all the sites s on the polymer chain(s). For two polymer chains of length N_{ω} we can write¹²⁰

$$f_{\alpha,\gamma,\text{tot}}(i,j) = e_{\alpha,\gamma,\text{tot}}(i,j) - 1$$

$$= \exp\left[-\beta \sum_{s=1}^{N_{\alpha}} \sum_{s'=1}^{N_{\gamma}} u_{\alpha,\gamma}(\mathbf{r}_{i,\alpha}(s), \mathbf{r}_{i,\gamma}(s'))\right] - 1$$

$$= -1 + \prod_{s}^{N_{\alpha}} \prod_{s'}^{N_{\gamma}} [f_{\alpha,\gamma}(\mathbf{r}_{i,\alpha}(s), \mathbf{r}_{j,\gamma}(s')) + 1]$$
(9)

This product is over all pairs of monomers s and s' and leads to all possible combinations of monomer pairs in the sum. The only exception is the part of the sum that is the product of the "ones" and cancels out with the -1 in the overall f-bond expression. Of particular interest to the RPA calculation are the terms that consist of only (1) a single factor $f_{\alpha,\gamma}(\mathbf{r}_{i,\alpha}(s), \mathbf{r}_{j,\gamma}(s'))$ that goes between any pair s and s' on chains s' and s' and s' products of two factors s' and s' and s' and s' products of two factors s' and s' and s' and s' products of two factors s' and s' and s' and s' products of two factors s' and s' and s' products of two factors s' and s' and s' and s' and s' products of two factors s' and s' an

$$f_{\alpha,\gamma,\text{tot}}(i,j) = -1 + \prod_{s}^{N_{\alpha}} \prod_{s'}^{N_{\gamma}} [f_{\alpha,\gamma}(\mathbf{r}_{i,\alpha}(s), \mathbf{r}_{j,\gamma}(s')) + 1]$$

$$\approx \sum_{s}^{N_{\alpha}} \sum_{s'}^{N_{\gamma}} f_{\alpha,\gamma}(\mathbf{r}_{i,\alpha}(s), \mathbf{r}_{j,\gamma}(s'))$$

$$+ \sum_{s}^{N_{\alpha}} \sum_{s'}^{N_{\gamma}} \sum_{s^{(2)}}^{N_{\alpha}} \sum_{s^{(3)}}^{N_{\gamma}} [f_{\alpha,\gamma}(\mathbf{r}_{i,\alpha}(s), \mathbf{r}_{j,\gamma}(s'))]$$

$$f_{\alpha,\gamma}(\mathbf{r}_{i,\alpha}(s^{(2)}), \mathbf{r}_{j,\gamma}(s^{(3)}))]$$

$$(10)$$

An important constraint we leave implicit is that the pair s, s' cannot be the same as $s^{(2)}$, $s^{(3)}$, which we will include explicitly in a more compact notation. This notation will leave implicit the spatial dependence of the functions f so that we only need to specify the species α and γ and the monomer indices s, s'; so for the rest of the manuscript we will replace $f_{\alpha,\gamma}(\mathbf{r}_{i,\alpha}(s),\mathbf{r}_{j,\gamma}(s')) \rightarrow f_{\alpha,\gamma|s,s'}$ so that the assumption in eq 10 is written as

$$f_{\alpha,\gamma,\text{tot}}(i,j) \approx \sum_{s,s'}^{N} f_{\alpha,\gamma|s,s'} + \sum_{s,s'\neq s^{(2)},s^{(3)}}^{N} f_{\alpha,\gamma|s,s} f_{\alpha,\gamma|s^{(2)},s^{(3)}}$$
(11)

We show in Appendix B that this expansion, when incorporated into the diagrams for the excess free energy, leads to a modified ring diagram

$$-\beta f_{exc} = \frac{1}{V} \left[\left(1 + \left(1 + \frac{1}{V} \right) + \left(\frac{1}{V} \right) + \frac{1}{V} \right) \right] + \dots \right]$$

Here, the orange lines correspond to ω -bonds that indicate correlations between spatially distinct sites. These diagrams have an interpretation similar to that of the analogous ring diagrams for molecular electrolytes, with each dashed Ψ -bond contributing a factor of $4\pi\lambda_{\rm B}z_{\alpha}z_{\beta}\psi(k)$ and each ρ -circle contributing $\rho_{\alpha}N_{\alpha}$. Now, however, the orange lines contribute an additional factor $S_{\alpha}(\mathbf{k})$. For a polymeric species modeled by a Gaussian chain, this factor is $S_{\alpha}(\mathbf{k}) = N_{\alpha}g_{{\rm D},\alpha}(k)$, where $g_{{\rm D}}(k) = \frac{2}{x^2}[e^{-x} + x - 1]$ is the Debye function where $x = R_{\rm g}^2k^2\cdot\frac{116,121}{x^2}$ However, it is possible in principle to use other single-molecule structure factors such as those for wormlike or rigid rod chains. Similar to the Debye–Hückel case, we can write out the excess free energy as follows

$$\beta f_{\text{exc}} = \frac{1}{2(2\pi)^3} \int d\mathbf{k} \left[-\frac{(\kappa^2 N g_{\text{D}}(k)\psi(k))^2}{2} + \frac{(\kappa^2 N g_{\text{D}}(k)\psi(k))^3}{3} - \frac{(\kappa^2 N g_{\text{D}}(k)\psi(k))^4}{4} + \cdots \right]$$

$$= \frac{1}{2(2\pi)^3} \int d\mathbf{k} [-\kappa^2 N g_{\text{D}}(k)\psi(k) + \ln[1 + \kappa^2 N g_{\text{D}}(k)\psi(k)]]$$
(12)

The details of this derivation are provided in Appendix B. The second half of this integral is the same result described in Qin and de Pablo, 77 which is that $\beta f_{\rm exc} \nu_0 = \frac{\nu_0 \kappa^{3/2}}{3^{1/4} \pi b^{3/2}}$. The first term of the integral is divergent and differs from the result derived by Qin and de Pablo. This term is linear in density (via the κ^2 contribution) so it is thermodynamically irrelevant and can be interpreted as the "self-energy" of a polymer chain. A similar expression can be obtained upon extending this calculation to include salt, leading to the following expression

$$\beta f_{\text{exc}} \nu_0 = \frac{\nu_0}{2(2\pi)^3} \int d\mathbf{k} [-4\pi\lambda_{\text{B}} (\rho_{\text{p}} N^2 g_{\text{D}}(k) + \rho_{\text{S}}) \psi(k) + \ln[1 + 4\pi\lambda_{\text{B}} (\rho_{\text{p}} N^2 g_{\text{D}}(k) + \rho_{\text{S}}) \psi(k)]]$$
(13)

This is, once more, essentially identical to classical results for RPA in polyelectrolyte coacervates. The can specifically compare this to the result given by Kudlay and Olvera de la Cruz, the which is identical to this expression. This result is also consistent with the more general expression derived by Qin and de Pablo. More generally, the connection between the RISM formalism and RPA in field theory is well-established in the literature, to the extent that it is possible to further extend this approach to systematically account for higher-order fluctuations in the polymer field theory. The coace of the c

■ EXCLUDED VOLUME IN RPA-BASED MODELS

The models considered so far rely on an expansion of the f-bond that separates out short-range interactions into the f_0 -bond while leaving the long-range contribution in the Ψ -bond, as shown in eq 49

$$f_{\alpha,\gamma} = f_{0,\alpha,\gamma} + (f_{0,\alpha,\gamma} + 1) \sum_{i=1}^{\infty} \frac{(-\beta u_{c,\alpha,\gamma})^i}{i!}$$
(14)

We then neglected any f_0 terms due to the long-range nature of the Coulomb potential $u_{c,\alpha,\gamma}$. However, the excluded volume contribution may be desirable for several reasons; most importantly, it can address the issue that the interaction energy diverges for completely overlapping particles (i.e., separated with zero distance). In addition, the excluded volume interactions between charged particles can become significant at high concentrations, in particular the densities seen in practice in coacervates. 23,28,30,104

One possible way to address the effect of excluded volume, from Kudlay and Olvera de la Cruz, is to change the effective potential considered in the Ψ -bonds such that $u_{c,\alpha,\gamma}(r) \to u_{c,\alpha,\gamma}(r) \left(1-e^{-b/r}\right)$. Here, b is a new length scale intended to represent the finite size of the salt and monomer charges in the solution. This has the desirable property that the energy of overlap does not diverge and instead goes to a constant value. This is effectively a soft excluded volume effect. The other

desirable aspect of this form of the potential is that it can be written in Fourier space 75,76

$$\hat{u}_{cO,\alpha,\gamma}(\mathbf{k}) = 4\pi z_{\alpha} z_{\gamma} \lambda_{\rm B} \psi_{\rm O}(\mathbf{k}) = \frac{4\pi \lambda_{\rm B} z_{\alpha} z_{\gamma}}{k^2 (1 + b^2 k^2)}$$
(15)

The quantity ψ_O can be simply substituted into the expression in eq 13, a modification that is explored at length in Kudlay et al. At reasonable concentrations, this result has significant implications on phase behavior, in particular, leading to a partitioning of salt out of the coacervate phase. 75,76

We note that this approach does not modify the diagrams considered by the cluster expansion and still considers only the ring diagrams. This is a general feature of the RPA approximation, even outside the context of electrostatics. For example, using $\psi(\mathbf{k}) = v$ represents an interaction of $u_{c,\alpha,\gamma}(\mathbf{r}) = v\delta(\mathbf{r})$, which then leads immediately to the Edwards result for the polymer solution free energy. This approach is still an improvement, of course, since it no longer neglects the effect of excluded volume that would otherwise be in the f_0 -bonds, yet there are other possible approaches.

An alternative to the above approach would be to explicitly include the non-Coulomb portion of the interaction potential, βu_s , as sums over some or all of the remaining non-ring diagrams. Perhaps the most trivial class of these diagrams are the diagrams without any Ψ -bonds and are the diagrams formed only from f_0 -bonds. This is schematically identical to the diagram expansion for the excess free energy using f-bonds, though neglecting any contribution due to the long-range electrostatics. If these f-bonds are single-site (i.e., each monomer is considered unconnected) and u_s is the hard-core potential then this contribution would be approximated by the well-known Carnahan—Starling result 119,124

$$\beta f_{\rm ex} \nu_0 = \frac{\varphi^2 (4 - 3\varphi)}{(1 - \varphi)^2} \tag{16}$$

A linear combination of the f_0 -bond diagrams and the RPA diagrams would be

$$-\beta f_{exc} = \frac{1}{V} \left[\begin{array}{c} \\ \\ \end{array} \right] + \begin{array}{c} \\ \\ \end{array} + \begin{array}{c} \\ \\ \end{array} + \cdots + \begin{array}{c} \\ \\ \end{array} + \begin{array}{c} \\ \\ \end{array}$$

We note that there is no overlap of these diagrams, so they can be additively combined. However, there is overlap between these diagrams and the Olvera de la Cruz approach. There, contributions from the self-site interactions would lead to ring diagrams that include some character of the excluded volume portion by its inclusion in the potential $u_{c,\alpha,\gamma}$. This means that there is some overlap with ring-like diagrams in the f_0 part of the expansion in the current case. Thus, these two approaches (including in the RPA vs adding on the Carnahan—Starling result) give rise to two different sets of slightly overlapping diagrams.

One aspect missing in the Carnahan–Starling result is the effect of connectivity between monomers. There are ways of accounting for the effect of excluded volume due to chains of connected beads, such as the Werthheim approach 125–127 used in models developed by Wang, et al. We will not explore this modification here but will instead account for the connectivity-based correlations by assuming a tunable factor in front of the excluded volume contribution to the free energy that we will discuss later.

ION PAIRING THEORY

Larson, Qin, and co-workers modified the RPA model of polyelectrolyte coacervation by accounting for effective chemical reactions between the charged species 36,39,99-101,109,128 that form ion pairs between polycation/polyanion monomers, cation/polyanion monomers, and anion/polycation monomers. While all pair combinations are typically explicitly included, 36,99,128 we start with the simpler case that does *not* include polycation/polyanion pairs 100

$$\beta f_{LQ} \nu_{0} = \frac{\varphi_{P+}}{N_{P+}} \ln \varphi_{P+} + \frac{\varphi_{P-}}{N_{P-}} \ln \varphi_{P-} + \varphi'_{+} \ln \varphi'_{+} + \varphi'_{-} \ln \varphi'_{-}$$

$$+ \varphi_{W} \ln \varphi_{W} + + \varphi_{P+} [\zeta_{+} \ln \zeta_{+} + (1 - \zeta_{+}) \ln \zeta_{+}]$$

$$+ \varphi_{P-} [\zeta_{-} \ln \zeta_{-} + (1 - \zeta_{-}) \ln \zeta_{-}] + + \zeta_{+} \varphi_{P+} \Delta G_{P+,-}$$

$$+ \zeta_{-} \varphi_{P-} \Delta G_{P-,+} + \frac{\nu_{0}}{4\pi^{2}}$$

$$\int dk [-4\pi \lambda_{B} (\rho_{P} N^{2} g_{D}(k) + \rho_{S}) \psi(k)$$

$$+ \ln[1 + 4\pi \lambda_{B} (\rho_{P} N^{2} g_{D}(k) + \rho_{S}) \psi(k)]]$$
(17)

This model builds on the RPA result by including a fraction of bound pairs, given by ζ_{\pm} , $^{36,99-101,109}$ between polyelectrolytes and the oppositely charged salt ions. These pairs contribute a free energy of binding $\Delta G_{P\pm,\mp}$ to the overall free energy, which serves as an empirical parameter in the third line of the above equation as well as a combinatoric entropy on the second line. $^{99-101,109}$ It is straightforward to extend this version of the model to account for the polycation—polyanion pairing. 36,99,128

This approach was originally developed to account for chemical bonding between the polyelectrolytes and their counterions such that the free energy of binding $\Delta G_{P+,\mp}$ is interpreted as a free energy of reaction and careful accounting of the number of counterions is included in the mixing entropy terms. 100 However, this model could alternatively be interpreted as reflecting concepts such as ion pairing and counterion condensation that are expected to emerge for polymers with high linear charge density 112,129,130 and are challenging to include explicitly in polymer field theory calculations. This is probably the simplest of the class of models that we will call "ion pairing" models (the other being the TM model discussed in the next section)¹⁰² and has had success in reproducing several experimental phase diagrams due to the flexibility in defining the effective binding free energies. 36,39 However, this also poses a challenge; there is no prescriptive way of choosing what is or is not included in this binding free energy $\Delta G_{P\pm,\pm}$ in the absence of an actual chemical reaction. To this end, we will show that systematic consideration of the cluster expansion provides a way to predict how this free energy emerges in high linear chargedensity polyelectrolyte coacervates, specifically in the absence of an actual ion binding reaction.

We recall the expression for the f-bond in eq 9

$$\begin{split} f_{\alpha,\gamma,\text{tot}}(i,j) &= -1 + \prod_{s}^{N_{\alpha}} \prod_{s'}^{N_{\gamma}} [f_{\alpha,\gamma|s,s,} + 1] \\ &= \sum_{s,s'} f_{\alpha,\gamma|s,s,} + \sum_{s,s'} \sum_{\neq s^{(2)},s^{(3)}} f_{\alpha,\gamma|s,s,} f_{\alpha,\gamma|s^{(2)},s^{(3)}} \\ &+ \sum_{s,s'} \sum_{\neq s^{(2)},s^{(3)}} \sum_{\neq s^{(4)},s^{(5)}} f_{\alpha,\gamma|s,s} f_{\alpha,\gamma|s^{(2)},s^{(3)}} f_{\alpha,\gamma|s^{(4)},s^{(5)}} + \cdots \end{split}$$

$$(18)$$

In the development of RPA, we used expansions of the first two terms (single and double factors of f) without considering the higher-order terms. In polymer field theory, it is possible to proceed beyond this approximation by expanding to higherorder field fluctuations using either diagrammatic expansion 12 or field theoretic simulations; ^{79–83} however, we instead choose to focus on the contribution of local particle-based correlations associated with the higher-order terms in eq 18, which cannot be readily treated via perturbative analyses. These higher-order terms are only non-zero when three interaction pairs are simultaneously occurring. For interaction sites on a polymer, however, this may be a possibility. To show how this may arise, we consider the interactions relevant to Qin and Larson, 36,99–101 where they specifically model polyelectrolyte/salt binding. We first consider only the interaction between a polycation and the surrounding salt species. If the polycation has a high linear charge density then it is relatively common to observe the following physical arrangement



Here, the charges flanking the closest interacting polycation—anion pair (at monomer s) also participate via a product $f_{P+,-|s-1}f_{P+,-|s}f_{P+,-|s+1}$. Here, we use the notation that the "nearest" monomer is s and omit the index for the monomeric anion. If we assume no other participants then we can write this product diagrammatically

$$f_{tot,P+,-}^{(3)} = \sum_{s} \left(\bigcap_{P+} \theta_{s,-} \right) \theta_{s,-}$$

Here, there are f-bonds between the orange (P+) and purple (-) species, denoted on the schematic explicitly. The summation is over all possible "center" monomers s, with the function $\theta_{s,-} = 1$ only when the salt ion is closest to s and $\theta_{s,-} = 0$ otherwise. We will discuss this function in more detail when we describe the practical choices in calculating these terms, but for now, we will contend that it is this function that specifies if a salt ion is "paired" with a polyelectrolyte monomer s. The area contained within the three orange ρ -circles alludes to the emergence of a three-density distribution function associated with all three monomers once the integrals over polymer degrees of freedom in the overall cluster expansion is performed. The diagram in this notation only accounts for the specific product of f-bonds and not the integration over the particle degrees of freedom, which we will explicitly indicate. This will help us work with this formalism going forward. Finally, the superscript (3) indicates this is only the three f-bond contribution, omitting the one- and two-f-bond terms that contribute primarily to the ring diagrams in the RPA calculation. We use this diagrammatic representation to calculate the polyelectrolyte-ion interactions

$$\frac{[\text{two-particle connected diagram}]_{P_{+,\pm}}^{(3)}}{V} = \sum_{\gamma=\pm} \frac{\rho_{P+} \rho_{\gamma}}{2V} \int \mathcal{D} \mathbf{r}_{P+} P_{P+}$$

$$\int d\mathbf{r}_{\gamma} \times \left[\sum_{s}^{N_{P+}} \{ f_{P+,\gamma|s-1} f_{P+,\gamma|s} f_{P+,\gamma|s+1} \} \right] = \frac{\rho_{P+}}{2V} \int \mathcal{D} \mathbf{r}_{P+} P_{P+}$$

$$\int d\mathbf{r}_{\pm} \left[\sum_{s}^{N_{P+}} \{ \rho_{-} \mathcal{A}_{P+,-} + \rho_{+} \mathcal{A}_{P+,+} \} \theta_{s,\pm} \right] \tag{19}$$

This expression accounts for the interaction between the polycation and *both* the anion and cations. Of course, it is possible to switch the sign of the polycation terms to obtain the

corresponding polyanion terms. Finally, we use, for example, $\mathcal{A}_{P+,-}$ to denote the cluster diagram associated with a set of three adjacent polycation monomers with an anion

$$A_{P+,-} = \bigcap_{P+}$$

We rewrite this term, rearranging the summations and integrals and invoking symmetry in the salt species $\rho_+ = \rho_- = \rho_+$

$$\begin{split} \frac{[\text{two-particle connected diagram}]_{P_{+,\pm}}}{V} &= \frac{\varphi_{P_{+}}}{N_{P_{+}}\nu_{0}} \sum_{s}^{N_{P_{+}}} \int^{*} \mathcal{D}\mathbf{r}_{P_{+}}P_{P_{+}} \\ &\int \!\! d\mathbf{r}_{\!\pm} \frac{\varphi_{\!\pm}}{2\nu_{0}} \{\mathcal{A}_{P_{+,-}} + \mathcal{A}_{P_{+,+}}\} \theta_{\!s,\pm} \end{split} \tag{20}$$

Here, we have made the replacements $\rho_{P+} \to \phi_{P+}/(N_{P+}\nu_0)$ and $\rho_{\pm} \to \phi_{\pm}/\nu_0$ to convert the number densities to volume fractions. We remove the density in the denominator by removing the translational degree of freedom in the first integral over polycation conformations, denoted with a *. If we assume that this integral is numerically small, we can approximate this with

$$\begin{split} & \frac{[\text{two-particle connected diagram}]_{P_{+,\pm}}}{V} \approx \frac{\varphi_{P+}}{N_{P+}\nu_0} \\ & \sum_{s}^{N_{P+}} \ln \left[1 + \frac{\varphi_{\pm}}{2\nu_0} \int^* \mathcal{D}\mathbf{r}_{P+}P_{P+} \int d\mathbf{r}_{\pm} \{\mathcal{A}_{P+,-} + \mathcal{A}_{P+,+}\} \theta_{s,\pm} \right] \\ & = \frac{\varphi_{P+}}{N_{P+}\nu_0} \ln \left[\left(1 + \frac{\varphi_{\pm}}{2\nu_0} \int^* \mathcal{D}\mathbf{r}_{P+}P_{P+} \int d\mathbf{r}_{\pm} \{\mathcal{A}_{P+,-} + \mathcal{A}_{P+,+}\} \theta_{s,\pm} \right)^{N_{P+}} \right] \end{split}$$

$$(21)$$

In this last step, we assumed that all of the monomers were equivalent. The form of the expression in the natural log can be thought of as the single-site partition function where the ion can be in two "states"; the near-chain state is described by the integral term, while the away-from-chain state is given by the one. This is reinforced by the $\theta_{s,\pm}$ factor, which enforces locality in the second, integral term. We then use the binomial theorem to rewrite as

$$\begin{split} & \frac{\text{[two-particle connected diagram]}_{P_{+,\pm}}}{V} \approx \frac{\varphi_{P+}}{N_{P+}\nu_{0}} \\ & \ln \Biggl[\sum_{N_{B}}^{N_{P+}} \frac{N_{P+}!}{N_{B}!(N_{P+} - N_{B})!} \\ & \left(\frac{\varphi_{\pm}}{2\nu_{0}} \int^{*} \mathcal{D}\mathbf{r}_{P+}P_{P+} \int d\mathbf{r}_{\pm} \{\mathcal{A}_{P+,-} + \mathcal{A}_{P+,+}\} \theta_{s,\pm} \right)^{N_{B}} \Biggr] \\ & \approx \frac{\varphi_{P+}}{N_{P+}\nu_{0}} \\ & \ln \Biggl[\frac{N_{P+}!}{N_{B}!(N_{P+} - N_{B}^{*})!} \\ & \left(\frac{\varphi_{\pm}}{2\nu_{0}} \int^{*} \mathcal{D}\mathbf{r}_{P+}P_{P+} \int d\mathbf{r}_{\pm} \{\mathcal{A}_{P+,-} + \mathcal{A}_{P+,+}\} \theta_{s,\pm} \right)^{N_{B}^{*}} \Biggr] \end{aligned}$$

In this last step, we assume that there is a value of $N_{\rm B}^*$ that dominates the summation. This, along with the term related to

the polyanion, allows us to write the excess free energy associated with ion pairing

$$\begin{split} \beta f_{\text{LQ,exc}} \nu_0 &= -\frac{[\text{two-particle connected diagram}]_{p_{\pm,\pm}} \nu_0}{V} \\ &= \varphi_{p_+} [\xi_{p_+} \ln \xi_{p_+} + (1 - \xi_{p_+}) \ln (1 - \xi_{p_+})] \\ &+ \varphi_{p_-} [\xi_{p_-} \ln \xi_{p_-} + (1 - \xi_{p_-}) \ln (1 - \xi_{p_-})] \\ &- \varphi_{p_+} \xi_{p_+} \ln \varphi_{\pm} - \varphi_{p_-} \xi_{p_-} \ln \varphi_{\pm} + \varphi_{p_+} \xi_{p_+} \Delta G_{p_{+,\pm}} \\ &+ \varphi_{p_-} \xi_{p_-} \Delta G_{p_{-,\pm}} \end{split} \tag{23}$$

This expression, with a few minor differences, recovers eq 17. The first two terms account for the combinatoric entropy of counterion "binding", defining the fraction $\xi_{P+} = N_{\rm B}*/N_{P+}$. The subsequent terms account for the decrease in translational entropy for the bound states, which is related to the terms in eq 17 that account for the charge fraction-dependent terms in the mixing entropy. The final terms are the effective change in free energy of binding, $\Delta G_{P\pm,\pm}$, that are given by

$$\Delta G_{P\pm,\pm} = -\ln \left[\frac{1}{2\nu_0} \int^* \mathcal{D}\mathbf{r}_{P+} P_{P+} \int d\mathbf{r}_{\pm} \{\mathcal{A}_{P+,-} + \mathcal{A}_{P+,+}\} \theta_{s,\pm} \right]$$
(24)

The expression in the natural log can thus be interpreted as a bound state partition function, coming from the local electrostatic correlations beyond the electrostatic interactions included in the RPA formalism.

There are several primary differences with this result versus the original theory by Larson and Qin¹⁰⁰ but which we attribute to the differences in the original interpretation of the model as due to actual chemical binding versus the charge localization that we consider here. The first difference is that we do not explicitly include the fraction of un-paired charges into the RPA portion of the free energy. This is expected in the original theory because they are explicitly removing charges upon reacting, so the fraction reacted would both change—and be affected by the RPA fluctuations. 100 In our case, however, the charges remain present and contributing to the RPA. The second difference is similarly due to this difference in interpretation, which is that there is a subtle difference in how the translational entropy of the ions is treated. In the original theory, their mixing entropy is based on the number of "free" ions due to the binding reactions. ¹⁰⁰ In this version, there is a similar correction, but this only affects the prefactor of the natural log term and not the quantity in the natural log. Third, and critically for this paper, we now have an expression for the binding free energy $\Delta G_{P+,+}$ that is in principle able to be evaluated. In the original theory, this would instead be related to the reaction itself and would include both bond formation and changes in the electrostatic self-energy of the charges. 100 Finally, we note that the distinction between a true chemical bond versus charge localization has physical ramifications that are not expressed in either theory. For example, the presence of defined, chemical bonds would lead to gelation at high concentrations and frequent binding between polyelectrolytes as discussed in the next section. 131 While early models attempted to include some gelation-driven correlations, 75 ion pairing theories by Larson or Qin do not model this gelation explicitly and consequently do not make predictions about topology or changes in structure. In contrast, gelation is not necessarily expected in the absence of defined chemical bonds. Physical gelation is possible if local electrostatic interactions lead to long-lived ion pairs. In principle,

enumerating the number of ion pairs allows for an estimate of the gelation line.⁷⁵ However, in the current model, such an estimate does not account for the coupling between network connectivity and locations of ion pairs, nor does it make predictions for the lifetime of the ion pairs. Further elaborating and resolving these issues is not the focus of this work. In our charge localization interpretation, we use merely uses "clusters" as a way to book-keep the local electrostatic interactions.

■ POLYMER-POLYMER BINDING

We can make a prediction for a similar $\Delta G_{P_+,P_-}$ between the polymeric species. We write a similar expression for the two-particle diagram, only now considering both particles to be polymeric (and in the absence of salt). As a reminder, we are interested in products of three factors of f

$$f_{\alpha,\gamma,\text{tot}}^{(3)}(i,j) = \sum_{s,s'} \sum_{\neq s^{(2)},s^{(3)}} \sum_{\neq s^{(4)},s^{(5)}} f_{\alpha,\gamma|s,s} f_{\alpha,\gamma|s^{(2)},s^{(3)}} f_{\alpha,\gamma|s^{(4)},s^{(5)}}$$
(25)

We can write this in diagrammatic form in a similar fashion as for the polyelectrolyte/ion interactions

$$f_{tot,P+,P-}^{(3)} = \sum_{s,s'}^{N_{P\pm}} \left(\underbrace{\sum_{P+}^{P-}}_{P+} + \underbrace{\sum}_{} +$$

We consider all possible combinations of the three f-bonds between the three ρ -circles on each chain (purple circles for the polyanion monomers and orange circles for the polycation monomers). We also note that the double sum over all monomer indices indicates that we consider these local correlations on the entire set of monomers rather than just limiting local interactions to a single location along a given pair of polymer molecules. The $\theta_{s,s'}$ factor is similar to the earlier notation in that it considers the two monomers if each monomer is closest to the other. Because of these criteria, we also neglect the f-bonds that do not include either s or s' (i.e., no f-bonds between s-1 and s'-1). We introduce a short-hand for this extended series of diagrams

$$\mathcal{B}_{P+,P-}^{(1)} = \underbrace{\sum_{P_{-}}^{P_{-}}}_{P_{+}} = \underbrace{\sum_{P_{-}}^{P_{-}}}_{P_{+}} + \underbrace{\sum_{P_{-}}^{P_{-}}}_{P_{-}} + \underbrace{\sum_{P_{$$

This shorthand can be either symbolic, using $\mathcal{B}_{P+,P-}^{(1)}$ to denote that the interactions are between the oppositely charged polyelectrolytes and consider only a single point of ion pairing (i.e., between s and s'). We will generalize this later but now focus on only this set of diagrams. We can write the polyelectrolyte—polyelectrolyte interactions with the following expressions

$$\begin{split} &\frac{[\text{two-particle connected diagram}]_{P_{\pm},P_{\pm}}}{V} = \frac{\rho_{p_{+}}\rho_{p_{-}}}{2} \\ &\int^{*} \mathcal{D}\mathbf{r}_{p_{+}}P_{p_{+}} \int \mathcal{D}\mathbf{r}_{p_{-}}P_{p_{-}} \sum_{s}^{N_{p_{+}}} \sum_{s}^{N_{p_{-}}} \left\{\mathcal{B}_{p_{+},p_{-}}^{(1)} - \theta_{s,s'}\right\} \\ &+ \frac{\rho_{p_{+}}\rho_{p_{+}}}{2} \int^{*} \mathcal{D}\mathbf{r}_{p_{+}}P_{p_{+}} \int \mathcal{D}\mathbf{r}_{p_{+}}P_{p_{+}} \sum_{s}^{N_{p_{-}}} \sum_{s}^{N_{p_{+}}} \left\{\mathcal{B}_{p_{+},p_{+}}^{(1)} - \theta_{s,s'}\right\} \\ &+ \frac{\rho_{p_{-}}\rho_{p_{-}}}{2} \int^{*} \mathcal{D}\mathbf{r}_{p_{-}}P_{p_{-}} \int \mathcal{D}\mathbf{r}_{p_{-}}P_{p_{-}} \sum_{s}^{N_{p_{-}}} \sum_{s}^{N_{p_{-}}} \left\{\mathcal{B}_{p_{-},p_{-}}^{(1)} - \theta_{s,s'}\right\} \\ &= \frac{\varphi_{p_{+}}}{2N_{p_{+}}\nu_{0}} \sum_{s}^{N_{p_{+}}} \frac{\varphi_{p_{\pm}}}{\nu_{0}} \int^{*} \mathcal{D}\mathbf{r}_{p_{+}}P_{p_{+}} \\ &\int \mathcal{D}\mathbf{r}_{p_{\pm}}P_{p_{\pm}} \left\{\frac{1}{2}\mathcal{B}_{p_{+},p_{-}}^{(1)} + \mathcal{B}_{p_{+},p_{+}}^{(1)}\right\} \theta_{s,s'} \\ &+ \frac{\varphi_{p_{-}}}{2N_{p_{-}}\nu_{0}} \sum_{s}^{N_{p_{-}}} \frac{\varphi_{p_{\pm}}}{\nu_{0}} \int^{*} \mathcal{D}\mathbf{r}_{p_{+}}P_{p_{+}} \\ &\int \mathcal{D}\mathbf{r}_{p_{\pm}}P_{p_{\pm}} \left\{\frac{1}{2}\mathcal{B}_{p_{+},p_{-}}^{(1)} + \mathcal{B}_{p_{+},p_{+}}^{(1)}\right\} \theta_{s,s'} \end{aligned} \tag{26}$$

In the last step, we have simplified slightly by taking $N_{P+} = N_{P-} = N$ and $\phi_{P\pm} = \phi_{P+} = \phi_{P-}$. This expression is similar to the one given in eq 20, and indeed in a system with all interactions between the polyelectrolytes and salts, these results can be combined to yield an overall expression for the third-order contributions to the two-particle connected diagrams

$$\frac{[\text{two-particle connected diagram}]^{(3)}}{V} = \frac{\varphi_{P+}}{2N_{P+}\nu_{0}}$$

$$\sum_{s}^{N_{P+}} \int_{-\infty}^{*} \mathcal{D}\mathbf{r}_{P+}P_{P+} \left[\frac{\varphi_{P\pm}}{\nu_{0}} \int \mathcal{D}\mathbf{r}_{P\pm}P_{P\pm} \left\{ \frac{1}{2}\mathcal{B}_{P+,P-}^{(1)} + \mathcal{B}_{P+,P+}^{(1)} \right\} \theta_{s,s'} + \frac{\varphi_{\pm}}{2\nu_{0}} \int d\mathbf{r}_{\pm} \{\mathcal{A}_{P+,-} + \mathcal{A}_{P+,+}\} \theta_{s,\pm} \right]$$

$$+ \frac{\varphi_{P-}}{2N_{P-}\nu_{0}} \sum_{s}^{N_{P-}} \int_{-\infty}^{*} \mathcal{D}\mathbf{r}_{P-}P_{P-} \left[\frac{\varphi_{P\pm}}{\nu_{0}} \int \mathcal{D}\mathbf{r}_{P\pm}P_{P\pm} \right]$$

$$\left\{ \frac{1}{2}\mathcal{B}_{P+,P-}^{(1)} + \mathcal{B}_{P-,P-}^{(1)} \right\} \theta_{s,s'} + \frac{\varphi_{\pm}}{2\nu_{0}}$$

$$\int d\mathbf{r}_{\pm} \{\mathcal{A}_{P-,+} + \mathcal{A}_{P-,-}\} \theta_{s,\pm} \right]$$
(27)

Using the same procedures as for eqs 20–23, we can now write a version of the Larson–Qin excess free energy that accounts for polymer–polymer binding

$$\begin{split} \beta f_{\text{LQ,exc}} \nu_0 &= \varphi_{\text{p+}} [\xi_{\text{p+},\pm} \ln \xi_{\text{p+},\pm} + \xi_{\text{p+},\text{p\pm}} \ln \xi_{\text{p+},\text{p\pm}} \\ &+ (1 - \xi_{\text{p+},\pm} - \xi_{\text{p+},\text{p\pm}}) \ln (1 - \xi_{\text{p+},\pm} - \xi_{\text{p+},\text{p\pm}})] \\ &+ \varphi_{\text{p-}} [\xi_{\text{p-},\pm} \ln \xi_{\text{p-},\pm} + \xi_{\text{p-},\text{p\pm}} \ln \xi_{\text{p-},\text{p\pm}} \\ &+ (1 - \xi_{\text{p-},\pm} - \xi_{\text{p-},\text{p\pm}}) \ln (1 - \xi_{\text{p-},\pm} - \xi_{\text{p-},\text{p\pm}})] \\ &- \varphi_{\text{p+}} (\xi_{\text{p+},\pm} \ln \varphi_{\pm} + \xi_{\text{p+},\text{p\pm}} \ln \varphi_{\text{p\pm}}) \\ &- \varphi_{\text{p-}} (\xi_{\text{p-},\text{p\pm}} \ln \varphi_{\pm} + \xi_{\text{p-},\text{p\pm}} \ln \varphi_{\text{p\pm}}) \\ &+ \varphi_{\text{p+}} (\xi_{\text{p+},\pm} \Delta G_{\text{p+},\pm} + \xi_{\text{p+},\text{p\pm}} \Delta G_{\text{p+},\text{p\pm}}) \\ &+ \varphi_{\text{p-}} (\xi_{\text{p-},\pm} \Delta G_{\text{p-},\pm} + \xi_{\text{p-},\text{p\pm}} \Delta G_{\text{p-},\text{p\pm}}) \end{split}$$

The quantities for $\Delta G_{P+,\pm}$ and $\Delta G_{P-,\pm}$ are as defined in eq 24, and now, we can write a similar expression for, for example, $\Delta G_{P+,P+}$

$$\Delta G_{P+,P\pm} = -\ln \left[\frac{1}{\nu_0} \int^* \mathcal{D} \mathbf{r}_{P+} P_{P+} \right]$$

$$\int \mathcal{D} \mathbf{r}_{P\pm} P_{P\pm} \left\{ \frac{1}{2} \mathcal{B}_{P+,P-}^{(1)} + \mathcal{B}_{P+,P+}^{(1)} \right\} \theta_{s,s}$$
(29)

In the formalism given in eq 28, there is thus a combinatoric entropy of binding for both polymers with respect to the polymer-ion and polymer-polymer binding sites on both chains on the first two terms. The subsequent two terms account for the change in translational entropy upon undergoing a "binding" event, and finally the last two terms account for the free energies of binding that result from the local correlations. We can thus interpret the first three lines in eq 28 as pertaining to the random binding of the polyelectrolyte monomers to the oppositely charged salt and polyelectrolyte species, which could be to the same or different chains. The last line in eq 28 accounts for the free energy of these binding events, which are associated with the third-order cluster diagrams. Finally, as a reminder, these terms are in addition to both the mixing entropy and RPA terms that were also included in the Qin-Larson formalism 100 but can be formed from the standard ring diagrams that emerge from the first- and second-order products of f-bonds. Thus, these "ion binding" terms are an additional contribution to coacervate models, beyond the mixing entropy and RPA free energy contributions.

TM MODEL

Lytle and Sing developed a more elaborate ion-pairing theory that they dubbed the "transfer matrix model" of complex coacervation, which models the electrostatic interactions of a polyelectrolyte with its surroundings by mapping to a one-dimensional adsorption model. This mapping considered a test polyelectrolyte as a substrate, onto which the oppositely charged species (i.e., salt and polymer) was adsorbed. This was able to be solved, in some cases analytically, by the TM method that is commonly used to solve (for example) the one-dimensional Ising model or the Zimm—Bragg model of coil—helix transitions. They proposed the following free energy

$$\beta f_{\text{TM}} \nu_0 = \frac{\varphi_{P+}}{N_{P+}} \ln \varphi_{P+} + \frac{\varphi_{P-}}{N_{P-}} \ln \varphi_{P-} + \varphi_+ \ln \varphi_+ + \varphi_- \ln \varphi_-$$

$$- \frac{\varphi_{P+}}{2N_{P+}} \ln \Xi_{P+} - \frac{\varphi_{P-}}{2N_{P-}} \ln \Xi_{P-}$$

$$+ \zeta (\Lambda_{P+} \varphi_{P+} + \Lambda_{P+} \varphi_{P-} + \varphi_+ + \varphi_-)^3$$
(30)

The first four terms on the left-hand side are simply the mixing entropy contribution, and the last term is a phenomenological term to account for charge packing. 102 The interactions are accounted for in the fifth and sixth terms, which are the free energies of a test polyelectrolyte interacting with its surrounding, oppositely charged species. These oppositely charged species are modeled as "adsorbing" to monomer "sites" along the onedimensional polyelectrolyte chain such that each monomer can be in one of four states: paired with a salt ion (S), paired with a polymer charge (P' or P), or unpaired (0). The difference between states P' and P account for whether the polymer charge is the first in a run of interacting monomers (P') or one of the subsequent pairs in this run (P). With these states defined, we write a grand canonical partition function $\Xi_{P\pm} = \psi_i \mathcal{M}_{ij,\pm} \psi_i$ that accounts for these interactions using a "TM" $\mathcal{M}_{ii,\pm}$ that includes the Boltzmann factors associated with pairs of monomers in different adsorption states 102

$$\mathcal{M}_{ij,\pm} = \begin{bmatrix} SS & SP & SP' & S0 \\ PS & PP & PP' & P0 \\ P'S & P'P & P'P' & P'0 \\ 0S & 0P & 0P' & 00 \end{bmatrix} = \begin{bmatrix} A_{\pm} & A_{\pm} & A_{\pm} & A_{\pm} \\ 0 & E_{\pm} & F_{\pm} & 0 \\ B_{\pm} & B_{\pm} & B_{\pm} & B_{\pm} \\ D_{\pm} & D_{\pm} & D_{\pm} \end{bmatrix}$$
(31)

Removing the possibility of the "P" state leads to the Qin and Larson result, 100 where there is a single ion pair formed between the polyelectrolytes. However, it is very possible that "runs" form, where two chains remain aligned for several adjacent monomers on both chains. In this case, the model has monomer—monomer neighboring interactions that allow us to include increasing numbers of correlated charges. We can thus account for situations such as the following



The leftmost situation is what is accounted for in the Larson—Qin model, with the center and right configurations being conditionally probable on the likelihood of forming the left configuration. These diagrams represent along-the-chain "interactions", with the presence of the oppositely charged monomer being nearby being related to the state of the adjacent monomers.

CLUSTER DERIVATION OF TM MODEL

To derive this model, we first focus on the polycation—polyanion interactions and start from the expression used to derive the Qin—Larson model

[two-particle connected diagram] $_{P+,P-}^{(3)}$

$$V = \frac{\rho_{p+}\rho_{p-}}{2} \int_{-\infty}^{\infty} \mathcal{D}\mathbf{r}_{p+}P_{p+} \int_{-\infty}^{\infty} \mathcal{D}\mathbf{r}_{p-}P_{p-}f_{\alpha,\gamma,\text{tot}}^{(3)}$$

$$= \frac{\rho_{p+}\rho_{p-}}{2} \int_{-\infty}^{\infty} \mathcal{D}\mathbf{r}_{p+}P_{p+} \int_{-\infty}^{\infty} \mathcal{D}\mathbf{r}_{p-}P_{p-}$$

$$\sum_{s,s'} \sum_{\neq s^{(2)},s^{(3)}} \sum_{\neq s^{(4)},s^{(5)}} f_{\alpha,\gamma|s,s}f_{\alpha,\gamma|s^{(2)},s^{(3)}}f_{\alpha,\gamma|s^{(4)},s^{(5)}}$$
(32)

In the previous case, we narrowed down the set of three f-bond diagrams by considering only the monomers local to a site there the two polymer species are spatially close (using the $\theta_{s,s'}$ function). However, we will now consider the possibility that the flanking monomers are also nearby to their counterparts on the opposing chain. We then will need to consider a less local set of correlations extending further down the two chains for at least another monomer pair. We will distinguish these scenarios by the number of sequential paired charges, writing this with the following

[two-particle connected diagram] $_{P+,P-}^{(3)}$

$$\frac{V}{2} = \frac{\rho_{p+}\rho_{p-}}{2} \int_{-\infty}^{\infty} \mathcal{D}\mathbf{r}_{p+}P_{p+} \int \mathcal{D}\mathbf{r}_{p-}P_{p-} \\
\times \sum_{s,s'}^{N_{p+}^{*}} \{\mathcal{B}_{p+,p-}^{(1)}\Theta_{1} + \mathcal{B}_{p+,p-}^{(2)}\Theta_{2} + \mathcal{B}_{p+,p-}^{(3)}\Theta_{3} + \cdots\}$$
(33)

We have extended the notations for the cluster diagrams $\mathcal{B}_{P+,P-}^{(i)}$, beyond the series $\mathcal{B}_{P+,P-}^{(1)}$ that is associated with a single point of ion pairing. The upper index (i) relates to the number of ion pairs. For example, we can write the following

$$\mathcal{B}_{P+,P-}^{(2)} = \underbrace{\begin{array}{c} P_{-} \\ P_{+} \end{array}}_{P+} + \underbrace{\begin{array}{c} P_{-} \\ P_{-} \end{array}}_{+} + \underbrace{\begin{array}{c} P_{-}$$

These are the summation of all diagrams consisting of three f-bonds between monomers on nearby polyelectrolytes, considering two points of contact for $\mathcal{B}^{(2)}_{P+,P-}$ and three points of contact for $\mathcal{B}^{(3)}_{P+,P-}$. In eq 33, the relevant diagram depends on the physical arrangement of the particles through the factors Θ_i ; these factors establish the criteria for each diagram such that, for example, $\Theta_1 = (1-\theta_{s-1,s'-1})\theta_{s,s'}(1-\theta_{s+1,s'+1})$ indicates that there is only a single paired set of charges, locally. The index indicates the number of paired set of charges in a run, such that

$$\Theta_2 = (1 - \theta_{s-1,s'-1})\theta_{s,s}\theta_{s+1,s'+1}(1 - \theta_{s+2,s'+2})$$
(34)

$$\Theta_{3} = (1 - \theta_{s-1,s'-1})\theta_{s,s}\theta_{s+1,s'+1}\theta_{s+2,s'+2}(1 - \theta_{s+3,s'+3})$$
(35)

The criteria are selected so that the relevant geometries are mutually exclusive, that is, that the summation in eq 33 reflects a choice of cluster diagrams based on the length of the run of paired charges for a specific set of conformations visited by the path integrals. Finally, we note that there is an asterisk on the chain length $N_{P\pm}$ * in the summation over indices s and s'. This acknowledges that this summation limit will be decremented by

one depending on the cluster diagram, as clusters with >1 paired contact will have fewer available sets of indices (e.g. N_P-1 for $B_{P+,P-}^{(2)}$, and N_P-2 for $B_{P+,P-}^{(3)}$).

With these additional terms in the cluster expansion, we can write out the entire two-particle connected diagram consisting of 3 *f*-bonds. Including the clusters associated with the polymer—ion correlations

$$\frac{[\text{two-particle connected diagram}]^{(3)}}{V} = \frac{\rho_{P+}\rho_{\pm}}{2} \int^{*} \mathcal{D}\mathbf{r}_{P+}P_{P+}$$

$$\int d\mathbf{r}_{\pm} \sum_{s}^{N_{P+}} \{\mathcal{A}_{P+,-} + \mathcal{A}_{P+,+}\} \theta_{s,\pm} + \frac{\rho_{P-}\rho_{\pm}}{2} \int^{*} \mathcal{D}\mathbf{r}_{P-}P_{P-}$$

$$\int d\mathbf{r}_{\pm} \sum_{s}^{N_{P-}} \{\mathcal{A}_{P-,+} + \mathcal{A}_{P-,-}\} \theta_{s,\pm} + \frac{\rho_{P+}\rho_{P-}}{2} \int^{*} \mathcal{D}\mathbf{r}_{P+}P_{P+}$$

$$\int \mathcal{D}\mathbf{r}_{P-}P_{P-} \times \sum_{s,s'}^{N_{P\pm}^{*}} \{\mathcal{B}_{P+,P-}^{(1)}\Theta_{1} + \mathcal{B}_{P+,P-}^{(2)}\Theta_{2} + \mathcal{B}_{P+,P-}^{(3)}\Theta_{3}$$

$$+ \cdots \} + \frac{\rho_{P+}^{2}}{2} \int^{*} \mathcal{D}\mathbf{r}_{P+}P_{P+} \int \mathcal{D}\mathbf{r}_{P+}P_{P+}$$

$$\times \sum_{s,s'}^{N_{P+}^{*}} \{\mathcal{B}_{P+,P+}^{(1)}\Theta_{1} + \mathcal{B}_{P+,P+}^{(2)}\Theta_{2} + \mathcal{B}_{P+,P+}^{(3)}\Theta_{3} + \cdots \}$$

$$+ \frac{\rho_{P-}^{2}}{2} \int^{*} \mathcal{D}\mathbf{r}_{P-}P_{P-} \int \mathcal{D}\mathbf{r}_{P-}P_{P-}$$

$$\times \sum_{s,s'}^{N_{P-}^{*}} \{\mathcal{B}_{P-,P-}^{(1)}\Theta_{1} + \mathcal{B}_{P-,P-}^{(2)}\Theta_{2} + \mathcal{B}_{P-,P-}^{(3)}\Theta_{3} + \cdots \}$$

$$\times \sum_{s,s'}^{N_{P-}^{*}} \{\mathcal{B}_{P-,P}^{(1)}\Theta_{1} + \mathcal{B}_{P-,P-}^{(2)}\Theta_{2} + \mathcal{B}_{P-,P-}^{(3)}\Theta_{3} + \cdots \}$$

$$(36)$$

We can combine terms associated with the polycation and polyanion and also terms associated with the various conditions Θ_i

$$\begin{split} &\frac{\left[\text{two-particle connected diagram}\right]^{(3)}}{V} = \frac{\varphi_{P+}}{2N_{P+}\nu_{0}} \\ &\sum_{s}^{N_{P+}^{*}} \ln \left[1 + \frac{\varphi_{\pm}}{\nu_{0}} \int^{*} \mathcal{D}\mathbf{r}_{P+}P_{P+} \int d\mathbf{r}_{\pm} \{\mathcal{A}_{P+,-} + \mathcal{A}_{P+,+}\} \theta_{s,\pm} \right. \\ &+ \frac{\varphi_{P\pm}}{\nu_{0}} \left(\int^{*} \mathcal{D}\mathbf{r}_{P+}P_{P+} \int \mathcal{D}\mathbf{r}_{P\pm}P_{P\pm} \times \left\{ \frac{1}{2} \mathcal{B}_{P+,P-}^{(1)} + \mathcal{B}_{P+,P+}^{(1)} \right\} \Theta_{1} \right. \\ &+ \int^{*} \mathcal{D}\mathbf{r}_{P+}P_{P+} \int \mathcal{D}\mathbf{r}_{P\pm}P_{P\pm} \left\{ \frac{1}{2} \mathcal{B}_{P+,P-}^{(2)} + \mathcal{B}_{P+,P+}^{(2)} \right\} \Theta_{2} \\ &+ \int^{*} \mathcal{D}\mathbf{r}_{P+}P_{P+} \int \mathcal{D}\mathbf{r}_{P\pm}P_{P\pm} \left\{ \frac{1}{2} \mathcal{B}_{P+,P-}^{(3)} + \mathcal{B}_{P+,P+}^{(3)} \right\} \Theta_{3} + \cdots \right) \right] \\ &+ \frac{\varphi_{P-}}{2N_{P-}\nu_{0}} \sum_{s}^{N_{P-}^{*}} \ln \left[1 + \frac{\varphi_{\pm}}{\nu_{0}} \int^{*} \mathcal{D}\mathbf{r}_{P-}P_{P-} \right. \\ &+ \left. \int \mathcal{D}\mathbf{r}_{P\pm}P_{P\pm} \times \left\{ \frac{1}{2} \mathcal{B}_{P-,P+}^{(1)} + \mathcal{B}_{P-,P-}^{(1)} \right\} \Theta_{1} + \int^{*} \mathcal{D}\mathbf{r}_{P-}P_{P-} \right. \\ &+ \left. \int \mathcal{D}\mathbf{r}_{P\pm}P_{P\pm} \left\{ \frac{1}{2} \mathcal{B}_{P-,P+}^{(2)} + \mathcal{B}_{P-,P-}^{(2)} \right\} \Theta_{2} + \int^{*} \mathcal{D}\mathbf{r}_{P-}P_{P-} \right. \\ &+ \left. \int \mathcal{D}\mathbf{r}_{P\pm}P_{P\pm} \left\{ \frac{1}{2} \mathcal{B}_{P-,P+}^{(3)} + \mathcal{B}_{P-,P-}^{(3)} \right\} \Theta_{3} + \cdots \right) \right] \end{aligned} \tag{37}$$

To simplify this expression, we use the following definitions, written in this case for the polycation

$$A_{0,+} = \frac{1}{\nu_0} \int_{0}^{*} \mathcal{D} \mathbf{r}_{p_{+}} P_{p_{+}} \int_{0}^{*} d\mathbf{r}_{\pm} \{ \mathcal{A}_{P+,-} + \mathcal{A}_{P+,+} \} \theta_{s,\pm}$$
 binding similar than the order of takes would autor chain then
$$F_{+} = \frac{1}{\nu_0} \int_{0}^{*} \mathcal{D} \mathbf{r}_{p_{+}} P_{p_{+}} \int_{0}^{*} \mathcal{D} \mathbf{r}_{p_{\pm}} P_{p_{\pm}} \left\{ \frac{1}{2} \mathcal{B}_{P+,P-}^{(1)} + \mathcal{B}_{P+,P-}^{(2)} + \mathcal{B}_{P+,P+}^{(2)} \right\} \Theta_{1}$$
 (39) then
$$F_{+} = \frac{\int_{0}^{*} \mathcal{D} \mathbf{r}_{p_{+}} P_{p_{+}} \int_{0}^{*} \mathcal{D} \mathbf{r}_{p_{\pm}} P_{p_{\pm}} \left\{ \frac{1}{2} \mathcal{B}_{P+,P-}^{(2)} + \mathcal{B}_{P+,P+}^{(2)} \right\} \Theta_{2}}{\int_{0}^{*} \mathcal{D} \mathbf{r}_{p_{+}} P_{p_{+}} \int_{0}^{*} \mathcal{D} \mathbf{r}_{p_{\pm}} P_{p_{\pm}} \left\{ \frac{1}{2} \mathcal{B}_{P+,P-}^{(1)} + \mathcal{B}_{P+,P+}^{(1)} \right\} \Theta_{1}$$
 (40)
$$\frac{31. \text{ W}}{B = B}$$

$$E_{+} = \frac{\int^{*} \mathcal{D}\mathbf{r}_{p_{+}} P_{p_{+}} \int \mathcal{D}\mathbf{r}_{p_{\pm}} P_{p_{\pm}} \left\{ \frac{1}{2} \mathcal{B}_{P_{+},P_{-}}^{(3)} + \mathcal{B}_{P_{+},P_{+}}^{(3)} \right\} \Theta_{3}}{\int^{*} \mathcal{D}\mathbf{r}_{p_{+}} P_{p_{+}} \int \mathcal{D}\mathbf{r}_{p_{\pm}} P_{p_{\pm}} \left\{ \frac{1}{2} \mathcal{B}_{P_{+},P_{-}}^{(2)} + \mathcal{B}_{P_{+},P_{+}}^{(2)} \right\} \Theta_{2}}$$

$$(41)$$

This allows us to rewrite eq 37 more succinctly as

[two-particle connected diagram]⁽³⁾

$$V$$

$$= \frac{\varphi_{P+}}{2N_{P+}\nu_{0}} \ln[(1 + A_{0,+}\varphi_{\pm} + B_{0,+}\varphi_{P\pm} + B_{0,+}\varphi_{P\pm}F_{+} + B_{0,+}\varphi_{P\pm}F_{+} + B_{0,+}\varphi_{P\pm}F_{+}E_{+}^{2} + \cdots)N_{P+}^{*}]$$

$$+ \frac{\varphi_{P-}}{2N_{P-}\nu_{0}} \ln[(1 + A_{0,-}\varphi_{\pm} + B_{0,-}\varphi_{P\pm} + B_{0,-}\varphi_{P\pm}F_{-} + B_{0,-}\varphi_{P\pm}F_{-}E_{-} + B_{0,-}\varphi_{P\pm}F_{-}E_{-}^{2} \cdots)N_{P-}^{*}]$$

$$+ B_{0,-}\varphi_{P\pm}F_{-}E_{-} + B_{0,-}\varphi_{P\pm}F_{-}E_{-}^{2} \cdots)N_{P-}^{*}]$$

$$(42)$$

Here we make the assumption that once we get to the factor E_+ or E_- , then the ratios of the 3-pair to 2-pair integrals is the same as if we calculated 4-pair to 3-pair integrals, and so on. We justify this by noting that this is interpreted as "extending" a run of paired charged on neighboring polyelectrolytes and that this extension reflects a criteria for the local bond directions that should become independent of the length of the run.

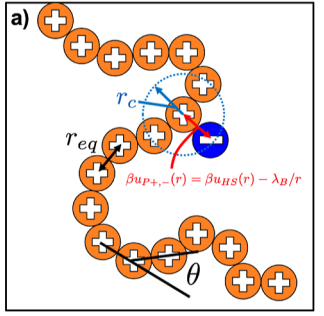
The resulting form for the excess free energy due to the thirdorder f-bond contributions in eq 42 is similar to the terms seen in eq 21 and can be interpreted as a series of independent "states" that can exist along the chain of N_{P+} * sites. The first term in the parenthesis (for each natural log term) is analogous to the vacant monomer site, the second term is related to pairing with the small molecule ions, and then the subsequent terms are related to polymer—polymer correlations between chains that are singly, doubly, triply, and quadruply bound in a manner analogous to the above schematic. However, this picture is complicated by the different number of monomer sites involved in the multiplybound states, and fewer of these can "fit" on a chain with N_{p_+} monomer sites. There is, thus, a longer chain of N_{P+} * states that is described by keeping the assumption of independence. We would prefer to, instead, choose only the number of states needed to accumulate N_{P+} monomer sites along the chain

The resolution to this issue is implied by our notation and leads to the TM formation. ¹⁰² If we step along a chain, we could come across a monomer that is paired to a monomer on the oppositely charged chain. At this moment, it could be a run characterized by a single set of paired monomers, and we start by assuming that option $(B_{0\pm}\phi_{P\pm})$. This does not require any special considerations for $N_{P\pm}$ since it is at this stage only a single

binding site. However, if the next monomer along the chain is similarly paired then now this is at least a doubly paired state. This requires the ratio F_\pm to essentially "replace" the integral by the one associated with $\mathcal{B}_{P\pm,P\pm}^{(2)}$. The relevant $N_{P^+}{}^*=N_P-1$ is decremented for this cluster because this doubly paired cluster takes up two monomer sites. However, in a TM formalism, we would obtain this cluster integral in two steps $(B_{0\pm}\phi_{P\pm}\times F_\pm)$, automatically accounting for this additional "space" along the chain. If the subsequent monomer along the chain is also paired then we can obtain the cluster integral in three steps $(B_{0\pm}\phi_{P\pm}\times F_\pm\times E_\pm)$, and so on. The two-particle connected diagrams can thus be written using the TM formalism described in eqs 30 and 31. We merely use the definitions already given and $A=A_{0,\pm}\phi_\pm$, $B=B_{0,\pm}\phi_{P\pm}$, and D=1.

SIMULATION CALCULATION OF THE CLUSTER DIAGRAM VALUES

While the cluster diagrams allow us to connect molecular interactions to model parameters in both the TM and Qin–Larson theory, we do not expect it to be possible to determine these quantities analytically. We resort to using simple Monte Carlo (MC) simulations to obtain values for these parameters ¹³³ and show that they can provide reasonable estimations of the parameters used in both TM theory and Q–L theory. See schematic in Figure 1a,b for the simulation setups to account for



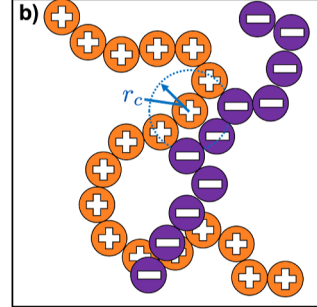


Figure 1. Simulation schemes for calculating cluster diagram values for (a) polymer—ion and (b) polymer—polymer interactions. Interactions between particles (e.g., $\beta u_{P+,-}(r)$ shown in a) are a combination of hard sphere repulsions $\beta u_{\rm HS}(r)$ and electrostatic interactions $\sim \lambda_{\rm B}/r$. Polymer chains are modeled with a harmonic bonding potential that keeps connected monomers at a distance $r_{\rm eq}$ and with a bending potential that is associated with the bond angle θ . Ion pairing criteria are given by the cutoff radius $r_{\rm cl}$ which is larger than the bead radius a. All parameters associated with these cutoffs and potentials are chosen to be the same as in our previous work, Lytle and Sing. 102

the polymer—ion and polymer—polymer interactions, respectively. We use a bead-spring MC model to obtain configurations of polymer segments with $N_{\rm sim}=9$ monomers at positions ${\bf r}_{ij}$ which feel a potential that only includes bonding and bending potentials

$$U = \frac{\kappa}{2} \sum_{\alpha} \sum_{i}^{N_{\alpha}-1} (|\mathbf{r}_{i+1,i,\alpha}| - r_{\text{eq}})^2 + \frac{\kappa_{\theta}}{2} \sum_{\alpha} \sum_{i}^{N_{\alpha}-2} \theta_{i,i+1,i+2,\alpha}^2$$
(43)

We have indicated a summation over all species α included in the simulation, and in this paper, we consider only two cases: (1) polyelectrolyte/ion and (2) polyelectrolyte/polyelectrolyte. Since our MC simulation is merely a scheme to perform the integrations described above, these calculations can simulta-

Table 1. TM Parameters

f_{c,P^+}	$f_{c,P-}$	$A_{0,+}$	$A_{0,-}$	$B_{0,+}$	$B_{0,-}$	$E_{\scriptscriptstyle +}$	E_	$F_{\scriptscriptstyle +}$	F_
1.0	1.0	19.4	19.4	23.7	23.7	0.42	0.42	0.87	0.87
0.9	0.9	13.5	13.5	14.7	14.7	0.35	0.35	0.82	0.82
0.8	0.8	9.23	9.23	7.15	7.15	0.29	0.29	0.66	0.66
0.7	0.7	5.62	5.62	3.52	3.52	0.22	0.22	0.66	0.66
0.6	0.6	3.14	3.14	1.37	1.37	-0.13	-0.13	0.51	0.51
0.5	0.5	1.85	1.85	0.35	0.35	-2.75	-2.75	0.24	0.24
0.9	1.0	13.5	19.4	18.33	23.7	0.36	0.42	0.80	0.87
0.8	1.0	9.23	19.4	13.58	23.7	0.36	0.42	0.81	0.87
0.7	1.0	5.62	19.4	9.92	23.7	0.33	0.42	0.75	0.87
0.6	1.0	3.14	19.4	6.64	23.7	0.36	0.42	0.72	0.87
0.5	1.0	1.85	19.4	4.86	23.7	0.16	0.42	0.57	0.87

neously consider like and opposite charges by simply changing the charge and separately calculating the respective cluster terms. More combinations could be considered if, for example, we were considering polyelectrolytes or electrolytes with asymmetric potentials. Multicomponent systems may also require more combinations of species. We consider parameters consistent with our prior work, $^{30,102-104,134}$ with a spring constant $\kappa=200k_{\rm B}T/a^2$ that is sufficiently large to make the bonds rod-like, and a bending constant $\kappa_{\theta}k_{\rm B}T=3.3$ that makes these chains semiflexible. The length scale a is the radius of the beads and is also related to the equilibrium bond distance $r_{\rm eq}$. Finally, we use periodic boundary conditions to limit the region of space over which we perform the cluster integrals using a value of L/a=25 that is far longer range than the cluster integral interactions due to the criteria defined by $\theta_{s,s'}$ and/or $\theta_{s,\pm}$.

To calculate the cluster diagrams, we must integrate over the possible conformations of the polymer chains and particles and account for the interactions. For the polycation/anion system, as an example, we numerically perform the integral

$$\begin{split} A_{0,P+} &= \frac{1}{\nu_{0}} \langle \theta_{s,\pm}(\mathcal{A}_{P+,-} + \mathcal{A}_{P+,+}) \rangle = \frac{L^{3}}{\tau(N_{P+} - 1)} \\ &\sum_{i=0}^{\tau} \sum_{s=2}^{N_{P+}-1} \left[f_{p+,i}(s) - \mathbf{r}_{-,i} \right] \\ &\times f_{p+,-}(|\mathbf{r}_{P+,i}(s+1) - \mathbf{r}_{-,i}|) f_{p+,-}(|\mathbf{r}_{P+,i}(s-1) - \mathbf{r}_{+,i}|) \\ &+ f_{p+,+}(|\mathbf{r}_{P+,i}(s) - \mathbf{r}_{-,i}|) f_{p+,+}(|\mathbf{r}_{P+,i}(s+1) - \mathbf{r}_{+,i}|) \\ &f_{p+,+}(|\mathbf{r}_{P+,i}(s-1) - \mathbf{r}_{+,i}|) \right] \theta_{s,\pm} \end{split}$$
(44)

Here, the summation is over τ MC steps indicated by the index i. As defined before, $f_{\alpha,\gamma}(r) = e^{-\beta u_{\alpha,\gamma}(r)} - 1$. We choose a form of the potential, $\beta u_{P+,-}(r) = \beta u_{HS}(r) - \lambda_B/r$, that includes a hardsphere part $\beta u_{HS}(r) = 0$ for r > 2a and $\beta u_{HS}(r) = \infty$ for $r \le 2a$, and an unscreened Coulomb part with a magnitude of $\beta u_{P+,-}(2a) = \lambda_B/(2a)$ at contact. This calculation depends on several choices, including the simulated chain structure via the values of κ , κ_θ , and r_{eq} and the choice of $\theta_{s,\pm}$. For this case, $\theta_{s,\pm} = 1$ only if s is the monomer closest to the ion. We also apply a cutoff r_{c} consistent with the criteria for pairing used in our prior work, 102,103 such that $\theta_{s,\pm} = 1$ only if $r_{s,\pm} < r_c$.

An analogous numerical calculation is performed for the other quantities $(B_{0,P\pm}, F_{\pm})$, and E_{\pm}) using a similar procedure, with the only difference being that for $\theta_{s,s'}$ we require that monomer s' is the closest to s and that the monomer s is closest to s' (i.e., they are the closest pair), in addition to that distance being $< r_c$.

We can also consider chains with a charge fraction $f_{\rm c} < 1$ to understand the connection between these third order contributions, the contributions of the RPA terms, and how they relate to linear charge density. To account for $f_{\rm c} < 1$, the evaluation of the integral given numerically in eq 44 (or the analogous calculations for the other quantities) can be performed over randomly chosen sequences of charged versus uncharged monomers.

We obtain the TM parameters for a wide variety of charge fractions for both the polycation and polyanion species and list them in Table 1. We have considered a series of different charge fractions and categorize them by (1) the fully charged polyelectrolytes, (2) symmetric polyelectrolytes with equal charge fractions $f_{c,P+} = f_{c,P-}$, and (3) only varying one of the polyelectrolyte charge fractions (in this case, $f_{c,P+}$). We will explore the ramifications of these different charge fractions on the phase diagram in the subsequent section but now note that the quantitative values were similar to those determined in our prior work for $f_{c,P+} = f_{c,P-} = 1$. This includes both the absolute values of A_0 and B_0 as well as the approximate relationship F = 2E, with the latter being originally proposed through combinatoric arguments. We also plot in Figure 2 the parameters A_0 and B_0 , with the latter calculated for both the

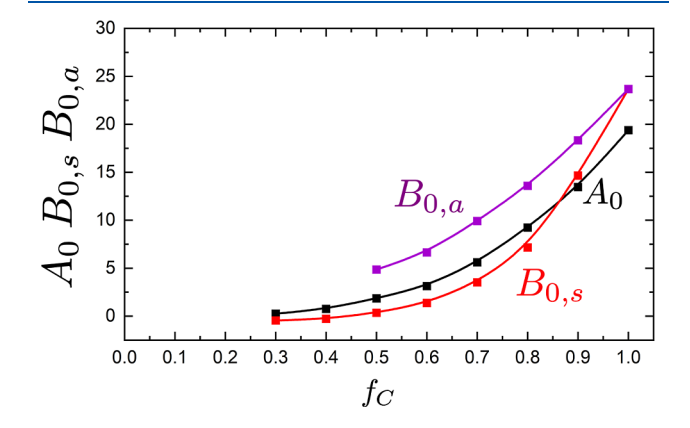


Figure 2. TM parameters A_0 and B_0 as a function of charge fraction f_C calculated by numerically evaluating expressions in eqs 38 and 39. For the polycation—polyanion parameter B_0 , we consider both the symmetric case $B_{0,s}$ where both chains have the same charge fraction $f_c < 1$ and the asymmetric case where one chain is fully charged while the other chain has a charge fraction $f_c < 1$. In all cases, the value of the parameter A_0 or B_0 decreases with decreasing charge fraction in a monotonic fashion, coinciding with a decrease in the importance of three-monomer interactions when charges become more spaced apart on average. Lines are included to guide the eye.

symmetric $(f_{c,P+} = f_{c,P-} = f_{c'} B_{0,s})$ and asymmetric $(f_{c,P+} = f_{c'} f_{c,P-} = 1, B_{0,a})$ cases. With decreasing $f_{c'}$ all of these parameters monotonically decrease due to the diminishing importance of correlated clusters at lower charge fractions. Understandably, the symmetric case exhibits a more pronounced decrease in B_0 as both interacting chains have fewer charges.

COMBINING CLUSTER DIAGRAMS TO MODEL COMPLEX COACERVATION

The benefit of using cluster diagrams as the foundation of these multiple coacervation models is that it is possible to systematically combine different theories that are complementary. To illustrate how this can be done, we point out that there are three types of contributions that can be combined without any overlap in meaning to develop a complex coacervate model. This includes (1) the RPA result for the excess free energy, which includes all ring diagrams, (2) the TM theory, which accounts for third-order multi-site interactions only between pairs of molecules, and (3) the hard core liquid contributions at the beyond-second order level, which are otherwise included in (1) and (2). We can diagramatically write a combined free energy that reflects these contributions

$$-\beta f_{exc} = \frac{1}{V} \left(\underbrace{\bigwedge_{P+}^{+}}_{P+} + \underbrace{\bigwedge_{P+}^{+}}_{P+} + \underbrace{\bigvee_{P+}^{+}}_{P+} + \underbrace{\bigvee_{P+}^{+}}_{+} + \underbrace{\bigvee_{P+}^{+}}_{+}$$

The first series of diagrams, underlined in red, are those involved with the TM theory. For brevity, we now implicitly include the integrations over the molecular degrees of freedom and the proximity constraints, and we explicitly include only the diagrams for the polycation species with the polyanion species remaining implied. These diagrams include both the polymersalt diagrams as well as the series of "ladder diagrams' that reflect the multi-site pairing between adjacent chains. These are thirdorder terms because the corresponding second- and first-order terms are included in the RPA portion of the free energy, which is given by the ring diagrams that are underlined in dark blue. For this work, we will use the Olvera de la Cruz model⁷⁶ since like the TM calculation, this incorporates some elements of the finite particle size in a pairwise fashion. Finally, the third contribution, underlined in light blue, is the third and higher-order diagrams associated with the hard core repulsions of all the species. We deliberately neglect the second-order contribution as it is already included in the RPA and TM portions of the calculation. We can use the models discussed in the previous section to write a free energy expression for coacervation using all of these diagrams

$$\begin{split} \beta f_{\rm c} \nu_0 &= \frac{\varphi_{P+}}{N_{P+}} \ln \varphi_{P+} + \frac{\varphi_{P-}}{N_{P-}} \ln \varphi_{P-} + \varphi_{+} \ln \varphi_{+} + \varphi_{-} \ln \varphi_{-} \\ &+ \varphi_{\rm W} \ln \varphi_{\rm W} - \frac{\varphi_{P+}}{2N_{P+}} \ln \Xi_{P+} - \frac{\varphi_{P-}}{2N_{P-}} \ln \Xi_{P-} \\ &+ \frac{\nu_0}{4\pi^2} \int \mathrm{d}k \ln[1 + 4\pi\lambda_{\rm B} (\rho_{P} N^2 g_{\rm D}(k) + \rho_{\rm S}) \psi(k)] \\ &+ \alpha \left[\frac{\varphi_{\rm tot}^2 (4 - 3\varphi_{\rm tot})}{(1 - \varphi_{\rm tot})^2} - 4\varphi_{\rm tot}^2 \right] \end{split} \tag{45}$$

The ordering of the terms in the excess free energy, after the mixing entropy terms, reflects the order of terms in the diagrams. First, the TM contributions are defined as above, with $\Xi_{P\pm} = \psi_i (\mathcal{M}_{P\pm}^{N_{P\pm}})_{ij} \psi_j$ and the cluster diagram-derived parameters. The subsequent RPA term is numerically evaluated, so we use a version where the thermodynamically irrelevant term linear in species densities ϕ_i is removed for convenience. The function $\psi(k) = \frac{1}{k^2(1+b^2k^2)}$ is the version from Olvera de la Cruz⁷⁶ that modifies the interaction potential to account for the finite size of the ion (related to the length scale b). Similarly, we can choose what we consider for $g_{\pi}(k)$ and for this work we

cruz that modifies the interaction potential to account for the finite size of the ion (related to the length scale b). Similarly, we can choose what we consider for $g_D(k)$, and for this work, we choose an approximate form for the wormlike chain that interpolates between the rigid rod and random walk limits 128,135,136

$$g_{\text{D,WLC}}(k) = \frac{e^{-kl_p/2}}{1 + k^2 N b l_p/6} + \frac{1 - e^{-kl_p/2}}{1 + k N_b/\pi}$$
(46)

This expression is used to be consistent with the semiflexible chain used in the simulations performed in this and previous works. Finally, the last two terms are associated with the Carnahan–Starling expression for the free energy of hard spheres; the second of these terms simply removes the quadratic contributions that would arise from the pairwise interactions already included in the TM and RPA terms. This is almost certainly an underestimation of this free energy due to the correlations associated with the connected polymer chains. We thus introduce the quantity α that is a tunable parameter that can correct for this approximation; this quantity is expected to be larger than the hard sphere fluid limit of $\alpha = 1$ but not significantly deviating from this limit.

In Figure 3a we plot the resulting phase diagram, determined from the free energy in eq 45 including all terms (TM, RPA, and C–S, black binodal) for $f_{c,P+} = f_{c,P-} = 1.0$. We first note that the phase diagram captures the key features of coacervation, as seen in similar simulations and experiments from the literature. This is unsurprising since the parameters we determined for this example are quantitatively close to those obtained from fitting to simulation data in the original TM theory. The main difference is that we are slightly over-predicting the binodal at the high- ϕ_S limit; this extends the critical point to higher salt concentrations, and we will suggest an explanation for this feature during our discussion of the limitations of this model later in this paper.

Because the TM, RPA, and C-S terms are all additive in the free energy, we can systematically turn on or off these contributions. To show how these expressions manifest, we plot in Figure 3a the predictions for phase separation using only the RPA and C-S terms, which is plotted with the blue curve and is a relatively small region of phase separation at low concentrations of ϕ_P and ϕ_S . While coacervation is predicted, it nevertheless exhibits a relatively weak phase separation that is quite different from the full phase diagram. Alternatively, we also show the phase diagram prediction using only the TM and C-S terms, which is plotted in red in Figure 3a and is far closer to the full phase diagram. Nevertheless, it still noticeably falls short of the full coacervate coexistence region. The TM theory thus dominates coacervate behavior, though the RPA-based attraction still plays a non-negligible role. Finally, we also plot in Figure 3a simulation data for the coacervate phase diagram from Lytle and Sing 102 that exhibits reasonable agreement with the theoretical predictions.

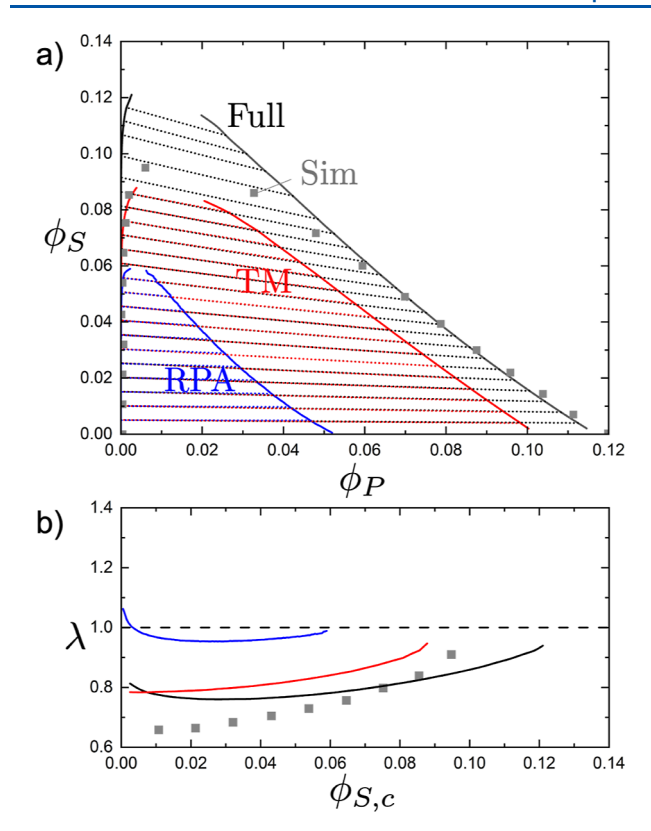


Figure 3. (a) Phase diagrams for a symmetric, fully charged polyelectrolyte coacervate using different approximations. The full phase diagram (black) uses the free energy expression given by eq 45 and includes terms associated with the TM theory, the RPA theory, and the Carnahan-Starling expression for the excluded volume. Also plotted are versions where the RPA portion is removed (red) and the TM portion is removed (blue) to show the relative contributions of both terms to the phase behavior. Also included are points from prior simulations that exhibit reasonable agreement with our model. 102 The only tunable parameter that we use is the quantity α that changes the magnitude of the excluded volume contribution to reflect the chain structure rather than the hard-sphere prediction given by Carnahan-Starling. (b) The salt partitioning coefficient λ that relates the concentration of salt in the coacervate versus the supernatant. If λ > 1, then salt partitions preferentially to the coacervate, while if λ < 1, salt partitions preferentially to the supernatant. Quantities demonstrated for the same set of models as in (a), with the full coacervate model again exhibiting reasonable agreement with molecular simulation. Simulation points reproduced from ref 102, copyright 2017, with permission from the Royal Society of Chemistry.

The other feature that all variations of this theory exhibit is the negative slope of the tie lines, with salt typically partitioning preferentially into the supernatant phase. We demonstrate this by plotting the partitioning coefficient $\lambda = \phi_{S,c}/\phi_{S,s}$ versus $\phi_{S,c}$ in Figure 3b, where $\phi_{S,c}$ is the salt concentration in the coacervate phase and $\phi_{S,s}$ is the salt concentration in the supernatant phase. However, the strength of this partitioning varies, with the lowest λ as the concentration of the coacervate increases. This is conceptually consistent with prior work, which suggests that preferential partitioning to the supernatant is driven primarily by the excluded volume of the components in the dense coacervate phase. $^{28,30,72}_{S,0}$ However, there is also a low- $\phi_{S,c}$ increase in λ that is a feature of the RPA theory, $^{76,96}_{S,c}$ which is driven by fluctuation-induced attraction between the dense polyelectrolyte phase and the salt ions and is seen in RPA predictions in the absence of excluded volume. $^{76,96}_{S,0}$ Once more, we plot the simulation

predictions for λ from Lytle, et al.¹⁰² to demonstrate consistency with the theoretical results.

■ FLUCTUATION-DRIVEN VERSUS ION PAIRING-DRIVEN COACERVATION

The emerging consensus in the coacervate field is that different theoretical approaches are relevant in different physical situations, with the linear charge density of the polyelectrolytes being particularly important. Field theoretic and scaling approaches are thought to best describe low-linear-charge-density polymers, while charge correlations inherent to the TM and other ion pairing approaches are thought to best describe high-linear-charge-density polymers. By deriving these two approaches from a consistent starting point, we can systematically consider the role of linear charge density on the balance between ion pairing and fluctuation-driven attraction. Indeed, in our formalism, these two concepts are separable because they constitute summations over two distinct sets of diagrams. By comparing these contributions, we can evaluate where these various approximations are more or less dominant.

To account for linear charge fraction in our calculations, we modify both the RPA and the TM terms in the theory. For the RPA calculation, we use the classical modification that explicitly includes the linear charge fraction $f_{\rm C}^{77}$

$$\beta f_{\text{exc,RPA},\sigma} \nu_0 = \frac{\nu_0}{4\pi^2} \int dk \ln[1 + 4\pi \lambda_{\text{B}} (\rho_{\text{p}} N^2 f_{\text{C}}^2 g_{\text{D}}(k) + \rho_{\text{S}}) \psi(k)]$$
(47)

We also consider changes to the TM terms, as described in the previous section, where the parameters $A_{0,\pm}$, $B_{0,\pm}$, E_{\pm} , and F_{\pm} are calculated by randomly selecting monomers to be charged or uncharged to match with a given f_C . This changes the factors $f_{\alpha,\gamma}$ by removing the Coulomb portion of the interaction energy $\beta u_{\alpha,\gamma}$.

We plot in Figure 4a coacervate phase diagrams for a variety of charge fractions $f_{C,+} = f_{C,-} = f_C$ that are the same on both polyelectrolytes. As this charge fraction is decreased from the fully charged limit $f_{\rm C}$ = 1.0, the coexistence regime becomes considerably smaller. This is the expected result, which is that the electrostatic driving force for coacervation becomes weaker; this is true for both the RPA and the TM terms and is consistent with the prior literature. 30,43,72,95,111 As the two-phase region shrinks, the partitioning of the salt also begins to invert such that at the lowest phase-separating case ($f_C = 0.5$), the tie line slopes are predominantly positive such that there is more salt in the coacervate than in the supernatant. This is seen in Figure 4b as conditions where $\lambda > 1$. These same trends become weaker when one of the polyelectrolytes remains fully charged, and we plot phase diagram predictions in Figure 5a for a series where $f_{C,+}$ = 1.0 and $f_{\rm C,-}$ < 1.0; here, the trends are essentially the same except the two-phase region shrinks less and the tie lines (plotted in terms of λ in Figure 5b) exhibit only subtle changes away from the fully charged limit.

The change in tie lines from negatively to positively sloped with decreasing $f_{\mathbb{C}}$ can be attributed to the shift from where the TM contributions are dominant to where the RPA contributions are dominant as the RPA is known to exhibit preferential salt partitioning to the coacervate phase. To quantify this, we define a metric to compare the relative strength of coacervate formation due to the RPA versus the TM contributions to the theory. We choose to not compare the absolute magnitudes of their free energies as an arbitrary reference free energy could be added rendering any comparison moot. Instead, we choose to compare

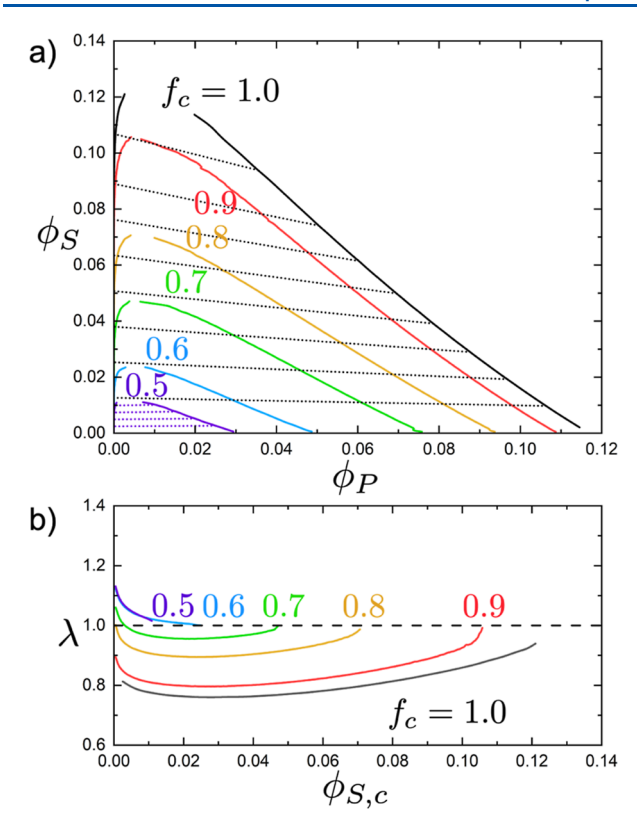


Figure 4. (a) Phase diagrams for symmetric polyelectrolyte coacervates with different linear charge densities, expressed in terms of the monomer charge fraction f_c . The fully charged case $f_c=1.0$ is the same as in Figure 3 and represents the largest extent of the two-phase region when compared with smaller values of $f_c=0.5-0.9$ indicated on the figure. As f_c decreases, the two-phase region shrinks considerably. Tie lines are shown for $f_c=1.0$ and $f_c=0.5$, which express the partitioning of salt between the phases. This is also shown in (b) in terms of the salt partitioning coefficient λ , which shows the transition from preferentially partitioning to the supernatant at large values of f_c to preferentially partitioning to the coacervate at small values of $f_c<0.7$.

the thermodynamically relevant second derivative quantities of the free energy contributions, which describes the strength of the driving force for phase separation due to each term in the free energy. We can write the comparison as

$$Q = \frac{\left(\frac{\partial^2 f_{\text{exc,TM}}(\varphi_{\text{S}} = 0)}{\partial \varphi_{\text{p}}^2}\right)}{\left(\frac{\partial^2 f_{\text{exc,RPA}}(\varphi_{\text{S}} = 0)}{\partial \varphi_{\text{p}}^2}\right)}$$
(48)

For simplicity's sake, we specifically choose to consider the zero-salt case for this paper as the driving force for phase separation becomes slightly more complicated for several components. We plot this comparison as a function of polymer concentration ϕ_P for several values of f_C in Figure 6.

We note several key observations about ϱ that provide insights into the various contributions to the coacervation free energy. First, the relative importance of the TM versus RPA portions of the free energy depends on the polymer concentration ϕ_P , with the latter being dominant only at the low- ϕ_P limit. This may be somewhat dubious as the RPA contribution to the excess free energy is known to overpredict phase separation in the dilute limit. Furthermore, the TM theory itself is known to be inaccurate in this limit. However, it is nevertheless physically

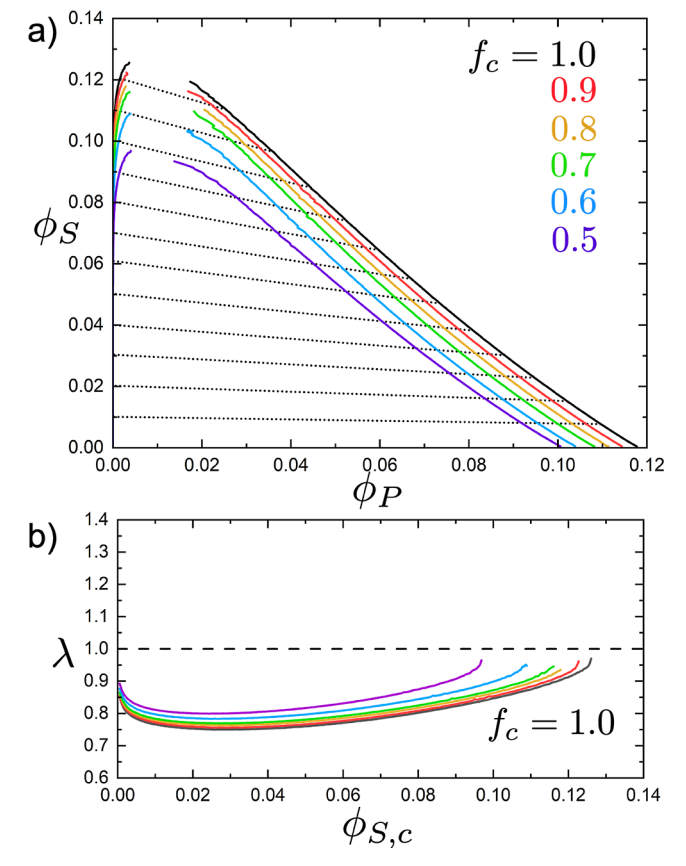


Figure 5. (a) Phase diagrams for polyelectrolyte coacervates where one of the polyelectrolytes has different linear charge densities, expressed in terms of the monomer charge fraction f_c of one of the polyelectrolyte species (the other polyelectrolyte has $f_c = 1$). The fully charged case $f_c = 1.0$ is the same as in Figures 3 and 4 and represents the largest extent of the two-phase region when compared with smaller values of $f_c = 0.5 - 0.9$ indicated on the figure. As f_c decreases, the two-phase region shrinks modestly compared to when both polyelectrolytes have varying charge densities. Tie lines are shown for $f_c = 1.0$, which express the partitioning of salt between the phases. This is also shown in (b) in terms of the salt partitioning coefficient λ, which shows only modest changes in salt partitioning upon varying f_c .

sensible that higher-order local correlations described by the TM theory become weaker when the concentration ϕ_P decreases, especially compared with the long-range contributions included in the RPA. At high charge density ($f_C > 0.7$), however, most of the ϕ_P regime is instead dominated by the TM theory, typically being $5-10\times$ the strength of the RPA contribution at typical coacervate densities. This is apparent in Figure 3a, where the TM-only phase diagram is much closer to the "full" result than the RPA-only phase diagram, and justifies the neglect of the RPA contribution to the theory in this limit.

At lower charge densities ($f_{\rm C} \leq 0.7$), however, the region where the RPA dominates grows significantly. At $f_{\rm C} = 0.5$, RPA dominates to relatively large values of ϕ_P , with $\varrho < 1$ until roughly $\phi_P \approx 0.07$. Notably, this is beyond the phase boundary for $f_{\rm C} = 0.5$ in Figure 4b such that coacervate is primarily driven by RPA. This transition to fluctuation-driven phase separation is also apparent in the salt partitioning, with $f_{\rm C} = 0.6$ being the point at which the value of λ starts to become consistently >1 in our model. This observation is broadly consistent with experimental data, wherein such a transition in behavior occurs around $f_{\rm C} = 0.5$; however, we also expect that these predictions

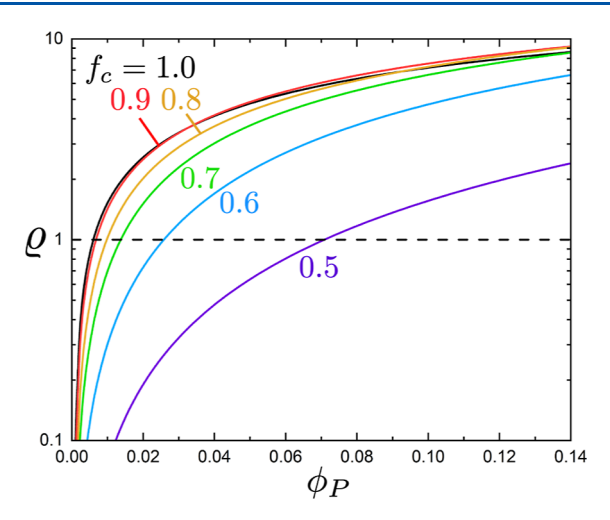


Figure 6. Dimensionless quantity ϱ describing the relative importance of the RPA vs TM contributions to the overall propensity for phase separation, plotted as a function of polymer concentration ϕ_P for several values of linear charge density $f_{\rm C}$. For all cases, the RPA contribution dominates at very low ϕ_P ($\varrho < 1$) though for highly charged polyelectrolytes (i.e., large $f_{\rm c}$), the TM dominates in most situations ($\varrho > 1$). The value of ϱ decreases considerably as $f_{\rm c} > 0.7$, which also coincides with the binodals for coacervation themselves shifting to lower values of ϕ_S . This quantifies the transition from ion pairing-dominated to fluctuation-dominated coacervation.

are sensitive to specific model parameters and that any prediction for the transition from RPA-dominated to TM-dominated behavior will be situation-dependent.

DISCUSSION AND CONCLUSIONS

In this paper, we have used a common starting point—a cluster expansion representation of the excess free energy—to show the relationships between several theoretical approaches to coacervation. The focus has been on two essentially orthogonal sets of cluster diagrams; the first is the set of "ring" diagrams taken from the Mayer theory of ionic solutions and can be related to the RPA excess free energy for coacervation, 75–77 and the second is a set of ladder-like diagrams to account for higher-order interactions and leads to the TM theory of coacervation. A third set of diagrams is added to account for non-pairwise hard sphere packing correlations, an important component that is responsible for setting the location of the binodal and the salt partitioning. This yields several insights that we think provide important context for the wide range of coacervate theories in the community:

- This represents the first derivation of the TM theory from a partition function, providing a more fundamental statistical mechanical justification for the setup of this model. Quantities such as $A_{0,\pm}$ and $B_{0,\pm}$ that were previously parameterized from simulations 102,103 are now related to cluster integrals that directly consider the molecular interactions. We can now be clearer about the approximations made in this approach and systematically account for these approximations diagrammatically.
- The diagrammatic representation allows us to write theories with non-overlapping contributions to the free energy, combining both fluctuations, strong charge correlations, and hard-sphere packing terms without redundancy. This has led to a new theory of coacervation,

given in eq 45, that limits to both ion pairing and RPA-based models.

- We now have a quantity *Q* that can be evaluated to determine the relevant importance of the RPA versus TM terms. While our new theory of coacervation includes both terms, we can show that for standard simulation models (i.e., the fully charged restricted primitive model), the TM term is dominant. However, as the linear charge density is decreased, the RPA term eventually becomes dominant.
- Salt partitioning is shown to be dependent on the molecular parameters, exhibiting preferential partitioning to the supernatant phase in the high- f_c limit but preferential partitioning to the coacervate phase in the low- f_c limit. This coincides with the transition from TM-dominated to RPA-dominated coacervate behavior. However, this is likely due to the specific interactions and molecular parameters involved as the RPA-only result for $f_c = 1.0$ shows preferential partitioning to the supernatant in contrast to the lower- f_c case.
- The cluster diagram approach may provide a useful starting point for systematically incorporating sequence effects, multicomponent coacervates, and non-electrostatic interactions. For this last point, it is notable that this only requires incorporating short-ranged potentials directly into the cluster diagram calculations.

We think that this is a useful starting point for developing more sophisticated models of polyelectrolyte solutions. At a fundamental level, the model developed here suffers from the same issues as the limiting theories and will require further development. So, despite the extensive formalism considered here, we can identify several areas where these models could be refined further:

- The RPA result for coacervation is known to be qualitatively inaccurate for polyelectrolyte complexes at low concentrations, 81,131,136 overpredicting phase separation in this limit. Comparison of RPA to the full fluctuating field theory, for example, shows dramatic differences, 81 and this will also affect ϱ in this limit. In this situation, plots versus $\log \varphi_p$ instead of φ_p are needed to resolve the subtle differences that will arise at the low- φ_p limit.
- The TM result for coacervation is also known to be qualitatively inaccurate for polyelectrolyte complexes at low concentrations because it neglects longer along-thechain correlations between pairs of oppositely charged polyelectrolytes. A more complicated set of diagrams may be able to account for these correlations, connecting nonadjacent correlated clusters.
- The cluster diagrams for the TM result only account for interactions between the flanking monomers of the ion pairs. This was an arbitrary choice made for convenience, which could be relaxed to account for longer along-thechain interactions.
- Relatedly, these cluster diagrams considered triple products of f-bonds, and it is possible that quadruple (or higher-order) products are also non-negligible. This choice was similarly done for the sake of simplicity, but a more systematic study may refine our theoretical predictions and will likely be important for sequencedefined polymers where we have previously shown that

the along-the-chain effects can extend beyond neighboring interactions.

- The approximation invoked going from eqs 20 and 21, in which we assume that the cluster integral is ≪1 so that we can replace it with a natural log, is useful to connect to ion pairing theories by Qin and Larson ^{99,100,128} and eventually to the TM theory. ^{43,102-107} This is not necessary, however, and it would be possible to instead numerically evaluate the summation in eq 20.
- While we consider many of the models developed in the literature, the relationship of this cluster approach to (for example) liquid-state theory models^{72,96,97} would be a useful direction for future study.
- Our free energy expressions do not provide straightforward predictions for molecular correlations or structures that could be tested in simulation or experiment. Further development of this formalism to predict these structures, for example, using the tools of liquid state theory and PRISM, ¹¹⁹ would be an important advance.
- We incorporate the dielectric effects implicitly by inserting the aqueous phase dielectric constant to the expression for the Coulomb interaction. Recent work has shown that the temperature dependence of dielectric permittivity adds important entropic contributions to the complexation of polyelectrolytes.¹³⁷ This has important ramifications for the temperature dependence of coacervate phase behavior,^{41,137–139} which we do not consider in this paper.

Finally, in addition to these areas for further model development, we expect that this approach will allow us to consider different molecular models beyond the coarse-grained linear chains we consider here. In particular, we anticipate that it would be straightforward to adapt this formalism to polymers with non-linear architectures or models with more chemical detail.

APPENDIX A

Ring Diagrams and the Derivation of the Debye—Hückel Free Energy

In the main paper, we introduced a series of ring diagrams that utilize Ψ -bonds that lead to the Debye–Hückel free energy, $\beta f_{\rm exc} = -\kappa^3/(12\pi)$, showing only a brief outline of the derivation. We present it in more detail here.

To show how to perform this derivation, we re-write the *f*-bond by splitting up the energy into a hard-sphere portion and a Coulomb portion, $\beta u_{\alpha,\gamma} = \beta u_{\rm s} + \beta u_{\rm c,\alpha,\gamma}^{140}$

$$f_{\alpha,\gamma} = e^{-\beta u_{\alpha,\gamma}} - 1 = f_{0,\alpha,\gamma} + (f_{0,\alpha,\gamma} + 1)(e^{-\beta u_{c,\alpha,\gamma}} - 1)$$

$$= f_{0,\alpha,\gamma} + (f_{0,\alpha,\gamma} + 1) \sum_{i=1}^{\infty} \frac{(-\beta u_{c,\alpha,\gamma})^i}{i!}$$
(49)

Here, the Coulomb contribution is $\beta u_{c,\alpha,\gamma}(\mathbf{r}_{i,\alpha},\mathbf{r}_{j,\gamma}) = \lambda_{\mathrm{B}} z_{\alpha} z_{\gamma}/|\mathbf{r}_{i,\alpha} - \mathbf{r}_{j,\gamma}|$ and the hard sphere potential is $\beta u_{\mathrm{hs}}(\mathbf{r}_{i},\mathbf{r}_{j}) = 0$ if $|\mathbf{r}_{i} - \mathbf{r}_{j}| \geq \sigma$ and otherwise $\beta u_{\mathrm{hs}}(\mathbf{r}_{i},\mathbf{r}_{j}) = \infty$. This allows us to replace a given f-bond with one or zero f_{0} -bonds, and any number of interaction bonds (which we will call Ψ -bonds by writing $\Psi_{\alpha,\gamma}(\mathbf{r}_{i},\mathbf{r}_{j}) = -\beta u_{c,\alpha,\gamma}$); however, at least one bond must be present in a given diagram. For the pairwise diagram, this means that the diagrams are now

Here, we have denoted the f_0 bonds with solid lines and the Ψ -bonds with dashed lines. To write out some of these diagrams, the first diagram on the right is simply

$$\frac{[\text{first diagram}]}{V} = \sum_{\alpha,\gamma} \frac{\rho_{\alpha} \rho_{\gamma}}{2V} \int \int d\mathbf{r}_{i,\alpha} d\mathbf{r}_{j,\gamma} [e^{-\beta u_{s}} - 1]$$

$$= \sum_{\alpha,\gamma} 2\pi \rho_{\alpha} \rho_{\gamma} \int_{0}^{\sigma} dr r^{2} [-1]$$

$$= -\frac{2\pi \sigma^{3}}{3} \sum_{\alpha,\gamma} \rho_{\alpha} \rho_{\gamma}$$
(50)

This is related to the first virial coefficient for a hard-core gas⁷¹ and becomes small at extreme dilution. We note that the negative sign is due to the identification of the cluster expansion with $-\beta f_{\rm exc}$ such that this ultimately contributes to the overall free energy as a penalty. The second diagram is

$$\frac{[\text{second diagram}]}{V} = \sum_{\alpha,\gamma} \frac{\rho_{\alpha} \rho_{\gamma}}{2V} \iint d\mathbf{r}_{i,\alpha} d\mathbf{r}_{j,\gamma} \left[-\frac{z_{\alpha} z_{\gamma} \lambda_{B}}{|\mathbf{r}_{j,\gamma} - \mathbf{r}_{i,\alpha}|} \right]
= \frac{\left(\sum_{\alpha} \rho_{\alpha} z_{\alpha}\right)^{2}}{2V} \iint d\mathbf{r}_{1} d\mathbf{r}_{2} \left[-\frac{\lambda_{B}}{|\mathbf{r}_{1} - \mathbf{r}_{2}|} \right]$$
(51)

The second version of the expression combines the densities and valencies into a single sum, which becomes zero in an electroneutral system. This is true of many diagrams in this expansion because any odd factor of the valency z_{α} will sum to zero. The lowest-order set of terms where this is not the case are the so-called ring diagrams. The third diagram involves both types of bonds. Its expression is the same as the second diagram, but the inter-particle separation is restricted by the f_0 -bond. Such a restriction does not affect charge neutrality argument, so the third diagram vanishes. To generalize, we expect a diagram to vanish if any ρ -circle in the diagram is joined by only one Ψ -bond. The fourth diagram above is the first in this series

$$\frac{\text{[fourth diagram]}}{V} = \sum_{\alpha,\gamma} \frac{\rho_{\alpha} \rho_{\gamma}}{4V} \int \int d\mathbf{r}_{i,\alpha} d\mathbf{r}_{j,\gamma} \left[\frac{z_{\alpha}^{2} z_{\gamma}^{2} \lambda_{B}^{2}}{|\mathbf{r}_{j,\gamma} - \mathbf{r}_{i,\alpha}|^{2}} \right]
= \frac{\left(\sum_{\alpha} \rho_{\alpha} z_{\alpha}^{2}\right)^{2}}{4} \int \int d\mathbf{r}_{l} d\mathbf{r}_{2} \left[\frac{\lambda_{B}^{2}}{|\mathbf{r}_{2} - \mathbf{r}_{l}|^{2}} \right]$$
(52)

This term does not cancel out, and indeed this is true for all ring diagrams because there are an even number of bonds going into each circle. There is also an additional factor of 1/2 compared to the previous diagrams that is due to the combinatoric factor associated with the two Ψ -bonds.

Mayer ionic solution theory obtains the Debye–Hückel theory result by considering an infinite series of these diagrams ^{69,115}

$$-\beta f_{exc} = \frac{1}{V} \left[\bullet \rightarrow + \triangle + \Box + \cdots \right]$$

To help evaluate this series, we use the well-known result that the Fourier transform of 1/r is $4\pi/k^2$ to re-write the diagrams. We start with the first ring diagram

$$\begin{split} &\frac{[1\text{st ring diagram}]}{V} = \frac{\left(\sum_{\alpha} \lambda_{\text{B}} \rho_{\alpha} z_{\alpha}^{2}\right)^{2}}{4V} \int \int d\mathbf{r}_{1} d\mathbf{r}_{2} \frac{1}{|\mathbf{r}_{2} - \mathbf{r}_{1}|^{2}} \\ &= \frac{\left(\sum_{\alpha} \lambda_{\text{B}} \rho_{\alpha} z_{\alpha}^{2}\right)^{2}}{4} \int \int d\mathbf{r}_{1} d\mathbf{r}_{2} \frac{\delta(\mathbf{r}_{2} - \mathbf{r}_{1})}{|\mathbf{r}_{1}| |\mathbf{r}_{2}|} \\ &= \frac{\left(\sum_{\alpha} \lambda_{\text{B}} \rho_{\alpha} z_{\alpha}^{2}\right)^{2}}{4} \int \int d\mathbf{r}_{1} d\mathbf{r}_{2} \frac{1}{|\mathbf{r}_{1}| |\mathbf{r}_{2}|} \frac{1}{(2\pi)^{3}} \int d\mathbf{k} e^{i\mathbf{k}(\mathbf{r}_{2} - \mathbf{r}_{1})} \\ &= \frac{\left(\sum_{\alpha} \lambda_{\text{B}} \rho_{\alpha} z_{\alpha}^{2}\right)^{2}}{4(2\pi)^{3}} \int d\mathbf{k} \int d\mathbf{r}_{1} \frac{e^{i\mathbf{k}\mathbf{r}_{1}}}{|\mathbf{r}_{1}|} \int d\mathbf{r}_{2} \frac{e^{-i\mathbf{k}\mathbf{r}_{2}}}{|\mathbf{r}_{2}|} \\ &= \frac{\left(4\pi \sum_{\alpha} \lambda_{\text{B}} \rho_{\alpha} z_{\alpha}^{2}\right)^{2}}{4(2\pi)^{3}} \int d\mathbf{k} \psi(\mathbf{k}) \psi(-\mathbf{k}) \end{split} \tag{53}$$

In the last step, we made the definition that $\psi(\mathbf{k}) = \psi(-\mathbf{k}) = k^{-2}$. The second ring diagram is similar

$$\frac{[2\operatorname{nd ring diagram}]}{V} = -\frac{\left(\sum_{\alpha} \lambda_{\mathrm{B}} \rho_{\alpha} z_{\alpha}^{2}\right)^{3}}{6}$$

$$\iint d\mathbf{r}_{1} d\mathbf{r}_{2} d\mathbf{r}_{3} \frac{\delta(\mathbf{r}_{3} - \mathbf{r}_{2} - \mathbf{r}_{1})}{|\mathbf{r}_{2} - \mathbf{r}_{1}| |\mathbf{r}_{3} - \mathbf{r}_{2}| |\mathbf{r}_{3} - \mathbf{r}_{1}|}$$

$$= -\frac{\left(\sum_{\alpha} \lambda_{\mathrm{B}} \rho_{\alpha} z_{\alpha}^{2}\right)^{3}}{6} \iint d\mathbf{r}_{1} d\mathbf{r}_{2} d\mathbf{r}_{3} \frac{1}{|\mathbf{r}_{1}| |\mathbf{r}_{2}| |\mathbf{r}_{3}|} \frac{1}{(2\pi)^{3}}$$

$$\int d\mathbf{k} e^{i\mathbf{k} \cdot (\mathbf{r}_{3} - \mathbf{r}_{2} - \mathbf{r}_{1})} = -\frac{\left(\sum_{\alpha} \lambda_{\mathrm{B}} \rho_{\alpha} z_{\alpha}^{2}\right)^{3}}{6(2\pi)^{3}} \int d\mathbf{k} \int d\mathbf{r}_{1} \frac{e^{-i\mathbf{k} \cdot \mathbf{r}_{1}}}{|\mathbf{r}_{1}|}$$

$$\int d\mathbf{r}_{2} \frac{e^{-i\mathbf{k} \cdot \mathbf{r}_{2}}}{|\mathbf{r}_{2}|} \int d\mathbf{r}_{3} \frac{e^{i\mathbf{k} \cdot \mathbf{r}_{3}}}{|\mathbf{r}_{3}|} = -\frac{\left(4\pi \sum_{\alpha} \lambda_{\mathrm{B}} \rho_{\alpha} z_{\alpha}^{2}\right)^{3}}{6(2\pi)^{3}}$$

$$\int d\mathbf{k} \psi^{3}(\mathbf{k}) \tag{54}$$

We use the definition from earlier that $\kappa = (4\pi\lambda_{\rm B}\sum_i \rho_i z_i^2)^{1/2}$ to write out the excess free energy density

$$\beta f_{\text{exc}} = -\frac{\kappa^4}{4(2\pi)^3} \int d\mathbf{k} \psi^2(\mathbf{k}) + \frac{\kappa^6}{6(2\pi)^3} \int d\mathbf{k} \psi^3(\mathbf{k}) - \frac{\kappa^8}{8(2\pi)^3} \int d\mathbf{k} \psi^4(\mathbf{k}) + \cdots$$

$$= \frac{1}{2(2\pi)^3} \int d\mathbf{k} \left[-\frac{(\kappa^2 \psi(k))^2}{2} + \frac{(\kappa^2 \psi(k))^3}{3} - \frac{(\kappa^2 \psi(k))^4}{4} + \cdots \right]$$
(55)

Considering that $\ln(1+x) = x - x^2/2 + x^3/3 - x^4/4 +$, we can write

$$\beta f_{\text{exc}} = \frac{1}{2(2\pi)^3} \int d\mathbf{k} \left[\kappa^2 \psi(k) - \kappa^2 \psi(k) - \frac{(\kappa^2 \psi(k))^2}{2} + \frac{(\kappa^2 \psi(k))^3}{3} - \frac{(\kappa^2 \psi(k))^4}{4} - \dots \right] = \frac{1}{2(2\pi)^3}$$

$$\int d\mathbf{k} [-\kappa^2 \psi(k) + \ln[1 + \kappa^2 \psi(k)]]$$
(56)

If we define a quantity $\tilde{k} = k/\kappa$; then we can re-write the final integral as

$$\beta f_{\text{exc}} = -\frac{\kappa^3}{4\pi^2} \int_0^\infty d\tilde{k} \tilde{k}^2 [\tilde{k}^{-2} - \ln[1 + \tilde{k}^{-2}]] = -\frac{\kappa^3}{12\pi}$$
(57)

The final integral that can be evaluated is $\pi/3$ and leads directly to the Debye–Hückel expression for the excess free energy.

APPENDIX B

Cluster Diagram Derivation of the RPA

To explicitly show how the expansion in eq 10 is incorporated into diagrams for the excess free energy, let us consider a simple pairwise diagram for a system with only polyelectrolytes of length $N_{P+} = N_{P-} = N$

$$\frac{[2\text{-particle diagram}]}{V} = \sum_{\alpha,\gamma} \frac{\rho_{\alpha} \rho_{\gamma}}{2V} \int \mathcal{D} \mathbf{r}_{\alpha} P_{\alpha}$$

$$\int \mathcal{D} \mathbf{r}_{\gamma} P_{\gamma} \left[\sum_{s,s'}^{N} f_{\alpha,\gamma|s,s'} + \sum_{s,s' \neq s^{(2)},s^{(3)}}^{N} f_{\alpha,\gamma|s,s} f_{\alpha,\gamma|s^{(2)},s^{(3)}} \right] \tag{58}$$

As mentioned in the main text, the second summation now explicitly includes the constraint that the pairs of s, s' and $s^{(2)}$, $s^{(3)}$ cannot be the same and reintroduces the factors P_{α} that account for intramolecular connectivity. This calculation is not considerably different from previous versions of this 2-particle diagram, though now there are path integrals over all possible conformations of the two polyelectrolytes. This can be analyzed in the same way as for the small molecule electrolytes, in that we can consider the ring diagrams with Ψ -bonds between ρ -circles; however, now that monomers can be connected on the same polymers, these "rings" can include polymer segments. One interaction can be between monomers s and s', while the other interaction can be between a different pair of monomers $s^{(2)}$ and $s^{(3)}$; this comes from the term consisting of products of two fbonds. Conversely, it is also possible that s = s'' and $s^{(2)} = s^{(3)}$, which comes from the single f-bond factors. We indicate the possibility of having connections between dissimilar monomer sites in diagrams by including ω -bonds that indicate correlations between spatially distinct sites, which we denote with orange lines. For the ring expansion, we represent this as

$$-\beta f_{exc} = \frac{1}{V} \left(\bigcirc + \bigcirc + \bigcirc + \cdots \right)$$

Note that, if there are only individual sites per chain, the orange lines disappear and we revert to the Debye—Hückel ring diagrams. To show how these diagrams work, we can write out the first integral as the following, considering at first the no-salt case with chains of equal length N

$$\begin{split} &\frac{[\text{1st ring diagram}]}{V} \approx \frac{1}{2} \sum_{\alpha,\gamma} \frac{\lambda_{\rm B}^2 \rho_{\alpha} \rho_{\gamma}^2 z_{\alpha}^2 z_{\gamma}^2}{2V} \sum_{s}^{N_{\alpha}} \sum_{s'=s}^{N_{\gamma}} \sum_{s'=s}^{N_{\gamma}} \sum_{s'=s}^{N_{\gamma}} \int \mathcal{D} \mathbf{r}_{1,\alpha}^P \rho_{\alpha} \\ &\int \mathcal{D} \mathbf{r}_{2,\gamma}^P \rho_{\gamma}^2 \times \frac{1}{|\mathbf{r}_{2,\gamma}(s') - \mathbf{r}_{1,\alpha}(s)|} \frac{1}{|\mathbf{r}_{2,\gamma}(s^{(3)}) - \mathbf{r}_{1,\alpha}(s^{(2)})|} \\ &= \frac{1}{2} \sum_{\alpha,\gamma} \frac{\lambda_{\rm B}^2 \rho_{\alpha}^2 \rho_{\gamma}^2 z_{\alpha}^2 z_{\gamma}^2}{2V} \sum_{s}^{N_{\gamma}} \sum_{s'=s}^{N_{\gamma}} \sum_{s'=s}^{N_{\gamma}} \int d\mathbf{r}_{3} \int d\mathbf{r}_{4} \int \mathcal{D} \mathbf{r}_{1,\alpha}^2 \rho_{\alpha} \\ &\int \mathcal{D} \mathbf{r}_{2,\gamma}^2 \rho_{\gamma}^2 \times \frac{\delta[\mathbf{r}_{3} - (\mathbf{r}_{1,\alpha}(s) - \mathbf{r}_{1,\alpha}(s^{(2)}))] \delta[\mathbf{r}_{4} - (\mathbf{r}_{2,\gamma}(s') - \mathbf{r}_{2,\gamma}(s^{(3)}))]}{|\mathbf{r}_{2,\gamma}(s') - \mathbf{r}_{1,\alpha}(s')|} \\ &\frac{1}{|\mathbf{r}_{2,\gamma}(s') - \mathbf{r}_{1,\alpha}(s)|} |\mathbf{r}_{2,\gamma}(s^{(3)}) - \mathbf{r}_{1,\alpha}(s^{(2)})| \end{aligned} \tag{59}$$

For a polymer chain α , the probability that any given conformational path that has monomers s and $s^{(2)}$ separated by a

distance of \mathbf{r}_3 is given by the site—site correlation function $\omega_{\alpha,s,s}$ ⁽²⁾($|\mathbf{r}_3|$). The path integrals over chain conformations give rise to an averaged quantity

$$\int \mathcal{D}\mathbf{r}_{\alpha}P_{\alpha}\delta[\mathbf{r}_{3} - (\mathbf{r}_{\alpha}(s) - \mathbf{r}_{\alpha}(s^{(2)}))] = \langle \omega_{\alpha,s,s^{(2)}}(|\mathbf{r}_{3}|) \rangle$$
(60)

This is simply the Green's function for a segment of length $\Delta s = s - s^{(2)}$ spanning a vector \mathbf{r}_3 . This can be further combined with the sums over the values s and $s^{(2)}$

$$\Omega_{\alpha}(\mathbf{r}_{3}) = \frac{1}{N_{\alpha}} \sum_{s=1}^{N_{\alpha}} \sum_{s^{(2)}=1}^{N_{\alpha}} \langle \omega_{\alpha,s,s^{(2)}}(|\mathbf{r}_{3}|) \rangle$$
(61)

We note that the Fourier transform of this sum over the site site correlation functions Ω_{P_+} is the structure factor

$$S_{\alpha}(\mathbf{k}) = \hat{\Omega}_{\alpha}(\mathbf{k}) = \int d\mathbf{r}_{3} \Omega_{i}(\mathbf{r}_{3}) e^{-i\mathbf{k}\mathbf{r}_{3}} = N_{\alpha}g_{\mathrm{D},\alpha}(\mathbf{k})$$
(62)

The last equivalence assumes a Gaussian chain and invokes the Debye function $g_D(\mathbf{k}) = \frac{2}{x^2} [e^{-x} + x - 1],^{116,121}$ where $x = R_{\varphi}^2 k^2$. Using this expression, we can write the first ring diagram as

$$\frac{\left[1\text{st ring diagram}\right]_{P_{+},P_{-}}}{V} \approx \frac{1}{2} \sum_{\alpha,\gamma} \frac{\lambda_{\rm B}^{2} \rho_{\alpha} \rho_{\gamma} z_{\alpha}^{2} z_{\gamma}^{2}}{2} \int d\mathbf{r}_{1} \int d\mathbf{r}_{2}$$

$$\int d\mathbf{r}_{3} \int d\mathbf{r}_{4} \times \frac{N_{\alpha} N_{\gamma} \Omega_{\alpha}(\mathbf{r}_{3}) \Omega_{\gamma}(\mathbf{r}_{4}) \delta[\mathbf{r}_{4} - \mathbf{r}_{3} - \mathbf{r}_{2} - \mathbf{r}_{1}]}{|\mathbf{r}_{1}| |\mathbf{r}_{2}|}$$

$$= \frac{1}{2} \frac{\left(4\pi \lambda_{\rm B} \sum_{\alpha} \rho_{\alpha} N_{\alpha} z_{\alpha}^{2}\right)^{2}}{2(2\pi)^{3}} \int d\mathbf{k} N^{2} g_{\rm D}^{2}(\mathbf{k}) \psi^{2}(\mathbf{k}) \tag{63}$$

At the last step, we make the assumption that both chains are identical in length N, except that they have opposite charge valency. This result is a straightforward modification of the result from the Debye–Hückel expression in eq 53 and justifies the diagrams we indicated earlier—each Ψ -bond contributes a factor ψ , and each orange ω -bond contributes a factor $Ng_{\rm D}$. We note that the factors of N_{α} in the prefactor are important as they convert the number density of chains, ρ_{ν} to number densities of monomers. The factors $Ng_{\rm D}$ account for connectivity of ideal, Gaussian coils, and simplify to factors of unity as $N \to 1$. The next ring diagram is again similar

$$\frac{\left[2\text{nd ring diagram}\right]_{P+,P-}}{V} \approx -\frac{1}{2} \frac{\left(4\pi\lambda_{\text{B}}\sum_{\alpha}\rho_{\alpha}N_{\alpha}z_{\alpha}^{2}\right)^{3}}{3(2\pi)^{3}}$$

$$\int d\mathbf{k}N^{3}g_{\text{D}}^{3}(\mathbf{k})\psi^{3}(\mathbf{k}) \tag{64}$$

We can thus write down, in a similar fashion to the Debye— Hückel case, the expression for the excess free energy

$$\begin{split} \beta f_{\text{exc}} &= -\frac{\kappa^4 N^2}{4(2\pi)^3} \int d\mathbf{k} g_{\text{D}}^2(\mathbf{k}) \psi^2(\mathbf{k}) + \frac{\kappa^6 N^3}{6(2\pi)^3} \\ &\int d\mathbf{k} g_{\text{D}}^3(\mathbf{k}) \psi^3(\mathbf{k}) - \frac{\kappa^8 N^4}{8(2\pi)^3} \int d\mathbf{k} g_{\text{D}}^4(\mathbf{k}) \psi^4(\mathbf{k}) + \\ &\cdots &= \frac{1}{2(2\pi)^3} \int d\mathbf{k} \left[-\frac{(\kappa^2 N g_{\text{D}}(k) \psi(k))^2}{2} \right. \\ &+ \frac{(\kappa^2 N g_{\text{D}}(k) \psi(k))^3}{3} - \frac{(\kappa^2 N g_{\text{D}}(k) \psi(k))^4}{4} + \cdots \right] \\ &= \frac{1}{2(2\pi)^3} \int d\mathbf{k} [-\kappa^2 N g_{\text{D}}(k) \psi(k) \\ &+ \ln[1 + \kappa^2 N g_{\text{D}}(k) \psi(k)]] \end{split}$$
(65)

This is the result given in eq 12.

We can extend this calculation to include salt by modifying the various ring diagrams to include more than just the polycation and polyanion species. We write out more explicitly the summation in the first ring diagram

$$\begin{split} &\frac{[1\text{st ring diagram}]}{V} = \frac{(4\pi\lambda_{\rm B})^2}{4(2\pi)^3} \\ &\int \mathrm{d}\mathbf{k} [\rho_{\rm P+} N_{\rm P+}^2 z_{\rm P+}^2 g_{\rm D}(\mathbf{k}) + \rho_{\rm P-} N_{\rm P-}^2 z_{\rm P-}^2 g_{\rm D}(\mathbf{k}) + \rho_{\rm +} z_{\rm +}^2 + \rho_{\rm -} z_{\rm -}^2]^2 \\ &\psi^2(\mathbf{k}) = \frac{(4\pi\lambda_{\rm B})^2}{2(2\pi)^3} \int \! d\mathbf{k} [\rho_{\rm P} N^2 g_{\rm D}(\mathbf{k}) + \rho_{\rm S}]^2 \psi^2(\mathbf{k}) \end{split} \tag{66}$$

Subsequent ring diagrams will maintain similar patterns to the no-salt and Debye—Hückel cases, so we can write

$$\beta f_{\text{exc}} \nu_0 = \frac{\nu_0}{2(2\pi)^3} \int d\mathbf{k} [-4\pi \lambda_{\text{B}} (\rho_{\text{P}} N^2 g_{\text{D}}(k) + \rho_{\text{S}}) \psi(k) + \ln[1 + 4\pi \lambda_{\text{B}} (\rho_{\text{P}} N^2 g_{\text{D}}(k) + \rho_{\text{S}}) \psi(k)]]$$
(67)

This is the expression given in eq 13.

AUTHOR INFORMATION

Corresponding Author

Charles E. Sing — Department of Chemical and Biomolecular Engineering, University of Illinois, Urbana, Illinois 61801, United States; orcid.org/0000-0001-7231-2685; Email: cesing@illinois.edu

Author

Jian Qin — Department of Chemical Engineering, Stanford University, Stanford, California 94305, United States; orcid.org/0000-0001-6271-068X

Complete contact information is available at: https://pubs.acs.org/10.1021/acs.macromol.3c01020

Note

The authors declare no competing financial interest.

ACKNOWLEDGMENTS

The authors acknowledge stimulating discussions with Andrew Spakowitz. C.E.S. acknowledges the hospitality of the Stanford Chemical Engineering Department during his sabbatical as well as support by the National Science Foundation under grant no. DMR-1654158.

REFERENCES

- (1) Sing, C.; Perry, S. Recent progress in the science of complex coacervation. *Soft Matter* **2020**, *16*, 2885–2914.
- (2) Gucht, J. v. d.; Spruijt, E.; Lemmers, M.; Cohen Stuart, M. A. Polyelectrolyte complexes: bulk phases and colloidal systems. *J. Colloid Interface Sci.* **2011**, 361, 407–422.
- (3) Srivastava, S.; Tirrell, M. V. Advances in Chemical Physics; Rice, S. A., Dinner, A. R., Eds.; John Wiley and Sons: Hoboken, NJ, 2016.
- (4) Kizilay, E.; Kayitmazer, A. B.; Dubin, P. L. Complexation and coacervation of polyelectrolytes with oppositely charged colloids. *Adv. Colloid Interface Sci.* **2011**, *167*, 24–37.
- (5) Kayitmazer, A. B.; Seeman, D.; Minsky, B. B.; Dubin, P. L.; Xu, Y. Protein-polyelectrolyte interactions. *Soft Matter* **2013**, *9*, 2553–2583.
- (6) Obermeyer, A.; Mills, C.; Dong, X.; Flores, R.; Olsen, B. Complex coacervation of supercharged proteins with polyelectrolytes. *Soft Matter* **2016**, *12*, 3570–3581.
- (7) Cummings, C. S.; Obermeyer, A. C. Phase separation behavior of supercharged proteins and polyelectrolytes. *Biochemistry* **2018**, *57*, 314–323.
- (8) Wang, Y.; Kimura, K.; Huang, Q.; Dubin, P. L.; Jaeger, W. Effects of Salt on Polyelectrolyte-Micelle Coacervation. *Macromolecules* **1999**, 32, 7128–7134.
- (9) Wang, Y.; Kimura, K.; Huang, Q.; Dubin, P. L.; Jaeger, W. Effects of Salt on Polyelectrolyte-Micelle Coacervation. *Macromolecules* **1999**, 32, 7128–7134.
- (10) Bungenberg de Jong, H. G.; Kruyt, H. R. Coacervation (partial miscibility in colloid systems). *Proc. Koninklijke Nederl. Akademie Wetenschappen* **1929**, 32, 849–856.
- (11) Schmitt, C.; Turgeon, S. L. Protein/polysaccharide complexes and coacervates in food systems. *Adv. Colloid Interface Sci.* **2011**, *167*, 63–70.
- (12) Yeo, Y.; Bellas, E.; Firestone, W.; Langer, R.; Kohane, D. S. Complex Coacervates for Thermally Sensitive Controlled Release of Flavor Compounds. *J. Agric. Food Chem.* **2005**, *53*, 7518–7525.
- (13) Turgeon, S. L.; Schmitt, C.; Sanchez, C. Protein-polysaccharide complexes and coacervates. *Curr. Opin. Colloid Interface Sci.* **2007**, *12*, 166–178.
- (14) Johnson, N.; Wang, Y. Coacervate delivery systems for proteins and small molecule drugs. *Expet Opin. Drug Discov.* **2014**, *11*, 1829–1832.
- (15) Black, K. A.; Priftis, D.; Perry, S. L.; Yip, J.; Byun, W. Y.; Tirrell, M. Protein encapsulation via polypeptide complex coacervation. *ACS Macro Lett.* **2014**, *3*, 1088–1091.
- (16) Blocher McTigue, W. C.; Perry, S. Design rules for encapsulating proteins into complex coacervates. *Soft Matter* **2019**, *15*, 3089–3103.
- (17) Blocher, W.; Perry, S. Complex coacervate-based materials for biomedicine. WIREs Nanomed. Nanobiotech. 2017, 9, No. e1442.
- (18) Brangwynne, C. P.; Tompa, P.; Pappu, R. V. Polymer physics of intracellular phase transitions. *Nat. Phys.* **2015**, *11*, 899–904.
- (19) Das, R.; Ruff, K. M.; Pappu, R. Relating sequence encoded information to form and function of intrinsically disordered proteins. *Curr. Opin. Struct. Biol.* **2015**, 32, 102–112.
- (20) Banani, S. F.; Lee, H. O.; Hyman, A. A.; Rosen, M. K. Biomolecular condensates: organizers of cellular biochemistry. *Nat. Rev. Mol. Cell Biol.* **2017**, *18*, 285–298.
- (21) Lin, Y.-H.; Forman-Kay, J. D.; Chan, H. S. Theories for sequence-dependent phase behaviors of biomolecular condensates. *Biochemistry* **2018**, *57*, 2499–2508.
- (22) McCarty, J.; Delaney, K. T.; Danielsen, S. P. O.; Fredrickson, G. H.; Shea, J.-E. Complete phase diagram for liquid-liquid phase separation of intrinsically disordered proteins. *J. Phys. Chem. Lett.* **2019**, *10*, 1644–1652.
- (23) Spruijt, E.; Westphal, A. H.; Borst, J. W.; Cohen Stuart, M. A.; van der Gucht, J. Binodal compositions of polyelectrolyte complexes. *Macromolecules* **2010**, *43*, 6476–6484.
- (24) Spruijt, E.; Sprakel, J.; Cohen Stuart, M. A.; van der Gucht, J. Interfacial tension between a complex coacervate phase and its coexisting aqueous phase. *Soft Matter* **2010**, *6*, 172–178.

- (25) Spruijt, E.; Cohen Stuart, M. A.; van der Gucht, J. Linear Viscoelasticity of Polyelectrolyte Complex Coacervates. *Macromolecules* **2013**, *46*, 1633–1641.
- (26) Spruijt, E.; Sprakel, J.; Lemmers, M.; Stuart, M. A. C.; van der Gucht, J. Relaxation Dynamics at Different Time Scales in Electrostatic Complexes: Time-Salt Superposition. *Phys. Rev. Lett.* **2010**, *105*, 208301.
- (27) Spruijt, E.; Leermakers, F. A. M.; Fokkink, R.; Schweins, R.; van Well, A. A.; Cohen Stuart, M. A.; van der Gucht, J. Structure and dynamics of polyelectrolyte complex coacervates studied by scattering of neutrons, X-rays, and light. *Macromolecules* **2013**, *46*, 4596–4605.
- (28) Li, L.; Srivastava, S.; Andreev, M.; Marciel, A. B.; de Pablo, J. J.; Tirrell, M. V. Phase behavior and salt partitioning in polyelectrolyte complex coacervates. *Macromolecules* **2018**, *51*, 2988–2995.
- (29) Perry, S.; Li, Y.; Priftis, D.; Leon, L.; Tirrell, M. The effect of salt on the complex coacervation of vinyl polyelectrolytes. *Polymers* **2014**, *6*, 1756–1772.
- (30) Radhakrishna, M.; Basu, K.; Liu, Y.; Shamsi, R.; Perry, S. L.; Sing, C. E. Molecular Connectivity and Correlation Effects on Polymer Coacervation. *Macromolecules* **2017**, *50*, 3030–3037.
- (31) Hoffmann, K. Q.; Perry, S. L.; Leon, L.; Priftis, D.; Tirrell, M.; de Pablo, J. J. A Molecular View of the Role of Chirality in Charge-Driven Polypeptide Complexation. *Soft Matter* **2015**, *11*, 1525–1538.
- (32) Priftis, D.; Xia, X.; Margossian, K. O.; Perry, S. L.; Leon, L.; Qin, J.; de Pablo, J. J.; Tirrell, M. Ternary, tunable polyelectrolyte complex fluids driven by complex coacervation. *Macromolecules* **2014**, *47*, 3076–3085
- (33) Perry, S. L.; Leon, L.; Hoffmann, K. Q.; Kade, M. J.; Priftis, D.; Black, K. A.; Wong, D.; Klein, R. A.; Pierce, C. F.; Margossian, K. O.; Whitmer, J. K.; Qin, J.; de Pablo, J. J.; Tirrell, M.; et al. Chirality-selected phase behaviour in ionic polypeptide complexes. *Nat. Commun.* **2015**, *6*, 6052.
- (34) Priftis, D.; Laugel, N.; Tirrell, M. Thermodynamic characterization of polypeptide complex coacervation. *Langmuir* **2012**, 28, 15947–15957.
- (35) Priftis, D.; Tirrell, M. Phase behaviour and complex coacervation of aqueous polypeptide solutions. *Soft Matter* **2012**, *8*, 9396–9405.
- (36) Lou, J.; Friedowitz, S.; Qin, J.; Xia, Y. Tunable coacervation of well-defined homologous polyanions and polycations by local polarity. *ACS Cent. Sci.* **2019**, *5*, 549–557.
- (37) Li, L.; Srivastava, S.; Meng, S.; Ting, J.; Tirrell, M. Effects of non-electrostatic intermolecular interactions on the phase behavior of pH-sensitive polyelectrolyte complexes. *Macromolecules* **2020**, *53*, 7835–7844.
- (38) Li, L.; Rumyantsev, A.; Srivastava, S.; Meng, S.; de Pablo, J.; Tirrell, M. Effect of solvent quality on the phase behavior of polyelectrolyte complexes. *Macromolecules* **2021**, *54*, 105–114.
- (39) Friedowitz, S.; Lou, J.; Barker, K. P.; Will, K.; Xia, Y.; Qin, J. Looping-in complexation and ion partitioning in nonstoichiometric polyelectrolyte mixtures. *Sci. Adv.* **2021**, *7*, No. eabg8654.
- (40) Vieregg, J. R.; Lueckheide, M.; Marciel, A. B.; Leon, L.; Bologna, A. J.; Rivera, J. R.; Tirrell, M. V. Oligonucleotide-peptide complexes: Phase control by hybridization. *J. Am. Chem. Soc.* **2018**, *140*, 1632–1638
- (41) Ali, S.; Bleuel, M.; Prabhu, V. Lower Critical Solution Temperature in Polyelectrolyte Complex Coacervates. *ACS Macro Lett.* **2019**, *8*, 289–293.
- (42) Chang, L. W.; Lytle, T. K.; Radhakrishna, M.; Madinya, J. J.; Vélez, J.; Sing, C. E.; Perry, S. L. Sequence and entropy-based control of complex coacervates. *Nat. Commun.* **2017**, *8*, 1273.
- (43) Lytle, T. K.; Chang, L.-W.; Markiewicz, N.; Perry, S. L.; Sing, C. E. Designing Electrostatic Interactions via Polyelectrolyte Monomer Sequence. *ACS Cent. Sci.* **2019**, *5*, 709–718.
- (44) Marianelli, A. M.; Miller, B. M.; Keating, C. D. Impact of macromolecular crowding on RNA/spermine complex coacervation and oligonucleotide compartmentalization. *Soft Matter* **2018**, *14*, 368–378.

- (45) Rathee, V. S.; Zervoudakis, A. J.; Sidky, H.; Sikora, B. J.; Whitmer, J. K. Weak polyelectrolyte complexation driven by associative charging. *J. Chem. Phys.* **2018**, *148*, 114901.
- (46) Voets, I. K.; de Keizer, A.; Cohen Stuart, M. A. Complex coacervate core micelles. *Adv. Colloid Interface Sci.* **2009**, 147–148, 300–318.
- (47) Maarten Biesheuvel, P.; Cohen Stuart, M. A.; Fokkink, R. G. Electrostatic Free Energy of Weakly Charged Macromolecules in Solution and Intermacromolecular Complexes Consisting of Oppositely Charged Polymers. *Langmuir* **2004**, *20*, 2785–2791.
- (48) Cohen Stuart, M. A.; Besseling, N. A. M.; Fokkink, R. G. Formation of micelles with complex coacervate cores. *Langmuir* **1998**, *14*, 6846–6849.
- (49) Srivastava, S.; Andreev, M.; Levi, A. E.; Goldfeld, D. J.; Mao, J.; Heller, W. T.; Prabhu, V. M.; de Pablo, J. J.; Tirrell, M. V. Gel phase formation in dilute triblock copolyelectrolyte complexes. *Nat. Commun.* **2017**, *8*, 14131.
- (50) Krogstad, D. V.; Choi, S.-H.; Lynd, N. A.; Audus, D. J.; Perry, S. L.; Gopez, J. D.; Hawker, C. J.; Kramer, E. J.; Tirrell, M. V. Small angle neutron scattering study of complex coacervate micelles and hydrogels formed from ionic diblock and triblock copolymers. *J. Phys. Chem. B* **2014**, *118*, 13011–13018.
- (51) Hofs, B.; Voets, I.; de Keizer, A.; Cohen Stuart, M. Comparison of complex coacervate core micelles from two diblock copolymers or a single diblock copolymer with a polyelectrolyte. *Phys. Chem. Chem. Phys.* **2006**, *8*, 4242–4251.
- (52) Audus, D. J.; Gopez, J. D.; Krogstad, D. V.; Lynd, N. A.; Kramer, E. J.; Hawker, C. J.; Fredrickson, G. H. Phase behavior of electrostatically complexed polyelectrolyte gels using an embedded fluctuation model. *Soft Matter* **2015**, *11*, 1214–1225.
- (53) Marciel, A. B.; Srivastava, S.; Tirrell, M. V. Structure and rheology of polyelectrolyte complex coacervates. *Soft Matter* **2018**, *14*, 2454–2464.
- (54) Ting, J. M.; Wu, H.; Herzog-Arbeitman, A.; Srivastava, S.; Tirrell, M. V. Synthesis and assembly of designer styrenic diblock polyelectrolytes. *ACS Macro Lett.* **2018**, *7*, 726–733.
- (55) Srivastava, S.; Levi, A. E.; Goldfeld, D. J.; Tirrell, M. V. Structure, Morphology, and Rheology of Polyelectrolyte Complex Hydrogels Formed by Self-Assembly of Oppositely Charged Triblock Polyelectrolytes. *Macromolecules* **2020**, *53*, 5763–5774.
- (56) Johnson, N. R.; Wang, Y. Coacervate delivery systems for proteins and small molecule drugs. *Expet Opin. Drug Deliv.* **2014**, *11*, 1829–1832.
- (57) Meng, X.; Perry, S.; Schiffman, J. Complex Coacervation: Chemically Stable Fibers Electrospun from Aqueous Polyelectrolyte Solutions. *ACS Macro Lett.* **2017**, *6*, 505–511.
- (58) Danielsen, S.; Nguyen, T.; Fredrickson, G.; Segalman, R. Complexation of a Conjugated Polyelectrolyte and Impact on Optoelectronic Properties. *ACS Macro Lett.* **2019**, *8*, 88–94.
- (59) Shamoun, R. F.; Reisch, A.; Schlenoff, J. B. Extruded saloplastic polyelectrolyte complexes. *Adv. Funct. Mater.* **2012**, *22*, 1923–1931.
- (60) Schaaf, P.; Schlenoff, J. B. Saloplastics: Processing compact polyelectrolyte complexes. *Adv. Mater.* **2015**, *27*, 2420–2432.
- (61) Stewart, R. J.; Wang, C. S.; Shao, H. Complex coacervates as a foundation for synthetic underwater adhesives. *Adv. Colloid Interface Sci.* **2011**, *167*, 85–93.
- (62) Holder, K. M.; Smith, R. J.; Grunlan, J. C. A review of flame retardant nanocoatings prepared using layer-by-layer assembly of polyelectrolytes. *J. Mater. Sci.* **2017**, *52*, 12923–12959.
- (63) Parveen, N.; Jana, P. K.; Schönhoff, M. Viscoelastic Properties of Polyelectrolyte Multilayers Swollen with Ionic Liquid Solutions. *Polymers* **2019**, *11*, 1285.
- (64) Li, J.; van Ewijk, G.; van Dijken, D. J.; van der Gucht, J.; de Vos, W. M. Single-Step Application of Polyelectrolyte Complex Films as Oxygen Barrier Coatings. *ACS Appl. Mater. Interfaces* **2021**, *13*, 21844–21853.
- (65) Sing, C. E. Development of the modern theory of polymeric complex coacervation. *Adv. Colloid Interface Sci.* **2017**, 239, 2–16.

- (66) Overbeek, J. T. G.; Voorn, M. Phase separation in polyelectrolyte solutions. Theory of complex coacervation. *J. Cell. Comp. Physiol.* **1957**, 49. 7–26.
- (67) Michaeli, I.; Overbeek, J. T. G.; Voorn, M. Phase separation of polyelectrolyte solutions. *J. Polym. Sci.* 1957, 23, 443–450.
- (68) Flory, P. J. Principles of Polymer Chemistry; Cornell University Press: Ithaca, NY, 1953.
- (69) Debye, P.; Huckel, E. Theory of electrolytes. *Phys. Z* **1923**, 24, 185.
- (70) Qin, J.; Priftis, D.; Farina, R.; Perry, S. L.; Leon, L.; Whitmer, J.; Hoffmann, K.; Tirrell, M.; de Pablo, J. J. Interfacial tension of polyelectrolyte complex coacervate phases. *ACS Macro Lett.* **2014**, *3*, 565–568.
- (71) McQuarrie, D. A. Statistical Mechanics; University Science Books: Sausalito, 2000.
- (72) Perry, S. L.; Sing, C. E. Prism-based theory of complex coacervation: Excluded volume versus chain correlation. *Macromolecules* **2015**, *48*, 5040–5053.
- (73) Borue, V. Y.; Erukhimovich, I. Y. A statistical theory of globular polyelectrolyte complexes. *Macromolecules* **1990**, *23*, 3625–3632.
- (74) Castelnovo, M.; Joanny, J.-F. Complexation between oppositely charged polyelectrolytes: Beyond the Random Phase Approximation. *Eur. Phys. J. E: Soft Matter Biol. Phys.* **2001**, *6*, 377–386.
- (75) Kudlay, A.; Ermoshkin, A. V.; Cruz, M. O. d. l. Comoplexation of oppositely charged polyelectrolytes: effect of ion pair formation. *Macromolecules* **2004**, *37*, 9213–9241.
- (76) Kudlay, A.; Olvera de la Cruz, M. Precipitation of oppositely charged polyelectrolytes in salt solutions. *J. Chem. Phys.* **2004**, *120*, 404–412.
- (77) Qin, J.; de Pablo, J. J. Criticality and connectivity in macromolecular charge complexation. *Macromolecules* **2016**, 49, 8789–8800.
- (78) Rumyantsev, A. M.; Kramarenko, E. Y.; Borisov, O. V. Microphase separation in complex coacervate due to incompatibility between polyanion and polycation. *Macromolecules* **2018**, *51*, 6587–6601.
- (79) Lee, J.; Popov, Y. O.; Fredrickson, G. H. Complex coacervation: A field theoretic simulation study of polyelectrolyte complexation. *J. Chem. Phys.* **2008**, *128*, 224908.
- (80) Riggleman, R. A.; Kumar, R.; Fredrickson, G. H. Investigation of the interfacial tension of complex coacervates using field-theoretic simulations. *J. Chem. Phys.* **2012**, *136*, 024903.
- (81) Delaney, K. T.; Fredrickson, G. H. Theory of polyelectrolyte complexation Complex coacervates are self-coacervates. *J. Chem. Phys.* **2017**, *146*, 224902.
- (82) Danielsen, S. P. O.; McCarty, J.; Shea, J.-E.; Delaney, K. T.; Fredrickson, G. H. Molecular design of self-coacervation phenomena in block polyampholytes. *Proc. Natl. Acad. Sci. U.S.A.* **2019**, *116*, 8224–8232.
- (83) Danielsen, S. P. O.; McCarty, J.; Shea, J.-E.; Delaney, K.; Fredrickson, G. Small ion effects on self-coacervation phenomena in block polyampholytes. *J. Chem. Phys.* **2019**, *151*, 034904.
- (84) Lin, Y.-H.; Song, J.; Forman-Kay, J.; Chan, H. Random-phase-approximation theory for sequence-dependent, biologically functional liquid-liquid phase separation of intrinsically disordered proteins. *J. Mol. Liq.* **2017**, 228, 176–193.
- (85) Das, S.; Amin, A. N.; Lin, Y.-H.; Chan, H. S. Coarse-grained residue-based models of disordered protein condensates: utility and limitations of simple charge pattern parameters. *Phys. Chem. Chem. Phys.* **2018**, 20, 28558–28574.
- (86) Lin, Y.-H.; Forman-Kay, J. D.; Chan, H. S. Sequence-Specific Polyampholyte Phase Separation in Membraneless Organelles. *Phys. Rev. Lett.* **2016**, *117*, 178101.
- (87) Wang, Z.; Rubinstein, M. Regimes of Conformational Transitions of a Diblock Polyampholyte. *Macromolecules* **2006**, *39*, 5897–5912.
- (88) Shusharina, N.; Zhulina, E.; Dobrynin, A.; Rubinstein, M. Scaling theory of diblock polyampholyte solutions. *Macromolecules* **2005**, *38*, 8870–8881.

- (89) Rubinstein, M.; Liao, Q.; Panyukov, S. Structure of Liquid Coacervates Formed by Oppositely Charged Polyelectrolytes. *Macromolecules* **2018**, *51*, 9572–9588.
- (90) Rumyantsev, A. M.; Zhulina, E. B.; Borisov, O. V. Complex Coacervate of Weakly Charged Polyelectrolytes: Diagram of States. *Macromolecules* **2018**, *51*, 3788–3801.
- (91) Rumyantsev, A. M.; de Pablo, J. J. Liquid crystalline and isotropic coacervates of semiflexible polyanions and flexible polycations. *Macromolecules* **2019**, *52*, 5140–5156.
- (92) Rumyantsev, A. M.; Jackson, N. E.; Johner, A.; de Pablo, J. J. Scaling Theory of Neutral Sequence-Specific Polyampholytes. *Macromolecules* **2021**, *54*, 3232–3246.
- (93) Danielsen, S. P. O.; Panyukov, S.; Rubinstein, M. Ion Pairing and the Structure of Gel Coacervates. *Macromolecules* **2020**, *53*, 9420–9442
- (94) Aponte-Rivera, C.; Rubinstein, M. Dynamic Coupling in Unentangled Liquid Coacervates Formed by Oppositely Charged Polyelectrolytes. *Macromolecules* **2021**, *54*, 1783–1800.
- (95) Rumyantsev, A. M.; Johner, A.; Tirrell, M. V.; de Pablo, J. J. Unifying Weak and Strong Charge Correlations within the Random Phase Approximation: Polyampholytes of Various Sequences. *Macromolecules* **2022**, *55*, 6260–6274.
- (96) Zhang, P.; Shen, K.; Alsaifi, N. M.; Wang, Z.-G. Salt partitioning in complex coacervation of symmetric polyelectrolytes. *Macromolecules* **2018**, *51*, 5586–5593.
- (97) Zhang, P.; Alsaifi, N. M.; Wu, J.; Wang, Z.-G. Polyelectrolyte complex coacervation: Effects of concentration asymmetry. *J. Chem. Phys.* **2018**, *149*, 163303.
- (98) Zhang, R.; Shklovskii, B. I. Phase diagram of solution of oppositely charged polyelectrolytes. *Phys. A* **2005**, 352, 216–238.
- (99) Salehi, A.; Larson, R. G. A Molecular Thermodynamic Model of Complexation in Mixtures of Oppositely Charged Polyelectrolytes with Explicit Account of Charge Association/Dissociation. *Macromolecules* **2016**, *49*, 9706–9719.
- (100) Friedowitz, S.; Salehi, A.; Larson, R. G.; Qin, J. Role of electrostatic correlations in polyelectrolyte charge association. *J. Chem. Phys.* **2018**, *149*, 163335.
- (101) Ghasemi, M.; Friedowitz, S.; Larson, R. Analysis of partitioning of salt through doping of polyelectrolyte complex coacervates. *Macromolecules* **2020**, *53*, 6928–6945.
- (102) Lytle, T. K.; Sing, C. E. Transfer matrix theory of polymer complex coacervation. *Soft Matter* **2017**, *13*, 7001–7012.
- (103) Lytle, T. K.; Sing, C. E. Tuning chain interaction entropy in complex coacervation using polymer stiffness, architecture, and salt valency. *Mol. Syst. Des. Eng.* **2018**, *3*, 183–196.
- (104) Lytle, T. K.; Salazar, A. J.; Sing, C. E. Interfacial properties of polymeric complex coacervates from simulation and theory. *J. Chem. Phys.* **2018**, *149*, 163315.
- (105) Sing, C. E. Micro- to macro-phase separation transition in sequence-defined coacervates. *J. Chem. Phys.* **2020**, *152*, 024902.
- (106) Madinya, J. J.; Chang, L.-W.; Perry, S. L.; Sing, C. E. Sequence-dependent self-coacervation in high charge-density polyampholytes. *Mol. Syst. Des. Eng.* **2019**, *5*, 632.
- (107) Liu, Y.; Santa Chalarca, C.; Carmean, R.; Olson, R.; Madinya, J.; Sumerlin, B.; Sing, C.; Emrick, T.; Perry, S. Effect of polymer chemistry on the linear viscoelasticity of complex coacervates. *Macromolecules* **2020**, *53*, 7851–7864.
- (108) Knoerdel, A. R.; Blocher McTigue, W. C.; Sing, C. E. Transfer Matrix Model of pH Effects in Polymeric Complex Coacervation. *J. Phys. Chem. B* **2021**, *125*, 8965–8980.
- (109) Ghasemi, M.; Friedowitz, S.; Larson, R. G. Overcharging of polyelectrolyte complexes: an entropic phenomenon. *Soft Matter* **2020**, *16*, 10640–10656.
- (110) Rathee, V. S.; Sidky, H.; Sikora, B. J.; Whitmer, J. K. Role of associative charging in the entropy-energy balance of polyelectrolyte complexes. *J. Am. Chem. Soc.* **2018**, *140*, 15319–15328.
- (111) Neitzel, A. E.; Fang, Y. N.; Yu, B.; Rumyantsev, A. M.; de Pablo, J. J.; Tirrell, M. V. Polyelectrolyte Complex Coacervation across a

- Broad Range of Charge Densities. Macromolecules 2021, 54, 6878-6890
- (112) Manning, G. S. Limiting laws and counterion condensation in polyelectrolyte solutions I. Colligative properties. *J. Chem. Phys.* **1969**, *51*, 924–933.
- (113) Ou, Z.; Muthukumar, M. Entropy and enthalpy of polyelectrolyte complexation: Langevin dynamics simulations. *J. Chem. Phys.* **2006**, *124*, 154902.
- (114) Yu, B.; Rumyantsev, A. M.; Jackson, N. E.; Liang, H.; Ting, J. M.; Meng, S.; Tirrell, M. V.; de Pablo, J. J. Complex coacervation of statistical polyelectrolytes: role of monomer sequences and formation of inhomogeneous coacervates. *Mol. Syst. Des. Eng.* **2021**, *6*, 790–804.
- (115) Mayer, J. E. The Theory of Ionic Solutions. *J. Chem. Phys.* **1950**, 18, 1426–1436.
- (116) Fredrickson, G. The Equilibrium Theory of Inhomogeneous Polymers; Oxford University Press, 2006.
- (117) Doi, M.; Edwards, S. The Theory of Polymer Dynamics; Clarendon Press, 1986; p 391.
- (118) Hill, T. L. An Introduction to Statistical Thermodynamics; Dover: New York, 1986.
- (119) Hansen, J. P.; McDonald, I. R. Theory of Simple Liquids; Elsevier: Boston, 2006.
- (120) Ladanyi, B. M.; Chandler, D. New type of cluster theory for molecular fluids: Interaction site cluster expansion. *J. Chem. Phys.* **1975**, 62, 4308–4324.
- (121) Rubinstein, M.; Colby, R. *Polymer Physics*; Oxford University Press: Oxford, 2003.
- (122) Morse, D. C. Diagrammatic analysis of correlations in polymer fluids: Cluster diagrams via Edwards' field theory. *Ann. Phys.* **2006**, 321, 2318–2389.
- (123) Ermoshkin, A. V.; Olvera De La Cruz, M. A modified random phase approximation of polyelectrolyte solutions. *Macromolecules* **2003**, 36, 7824–7832.
- (124) Carnahan, N. F.; Starling, K. E. Equation of State for Nonattracting Rigid Spheres. J. Chem. Phys. 1969, 51, 635–636.
- (125) Wertheim, M. Thermodynamic perturbation theory of polymerization. *J. Chem. Phys.* **1987**, *87*, 7323–7331.
- (126) Wertheim, M. S. Fluids with highly directional attractive forces. II. Thermodynamic perturbation theory and integral equations. *J. Stat. Phys.* **1984**, *35*, *35*–47.
- (127) Wertheim, M. S. Fluids with highly directional attractive forces. I. Statistical thermodynamics. *J. Stat. Phys.* **1984**, *35*, 19–34.
- (128) Friedowitz, S.; Qin, J. Reversible ion binding for polyelectrolytes with adaptive conformations. *AIChE J.* **2021**, *67*, No. e17426.
- (129) Muthukumar, M. Theory of counter-ion condensation on flexible polyelectrolytes: Adsorption mechanism. *J. Chem. Phys.* **2004**, *120*, 9343–9350.
- (130) Gonzalez-Mozuelos, P.; de la Cruz, M. O. Ion condensation in salt-free dilute polyelectrolyte solutions. *J. Chem. Phys.* **1995**, *103*, 3145–3157.
- (131) Muthukumar, M. 50th Anniversary Perspective: A Perspective on Polyelectrolyte Solutions. *Macromolecules* **2017**, *50*, 9528–9560.
- (132) Zimm, B. H.; Bragg, J. K. Theory of the Phase Transition between Helix and Random Coil in Polypeptide Chains. *J. Chem. Phys.* **1959**, *31*, 526–535.
- (133) Frenkel, D.; Smit, B. Understanding Molecular Simulation: From Algorithms to Applications; Academic Press: San Diego, CA, 2002.
- (134) Johnston, B. M.; Johnston, C. W.; Letteri, R. A.; Lytle, T. K.; Sing, C. E.; Emrick, T.; Perry, S. L. The effect of comb architecture on complex coacervation. *Org. Biomol. Chem.* **2017**, *15*, 7630–7642.
- (135) Ermoshkin, A. V.; Kudlay, A. N.; Olvera de la Cruz, M. Thermoreversible crosslinking of polyelectrolyte chains. *J. Chem. Phys.* **2004**, *120*, 11930–11940.
- (136) Shen, K.; Wang, Z.-G. Electrostatic correlations and the polyelectrolyte self energy. *J. Chem. Phys.* **2017**, *146*, 084901.
- (137) Chen, S.; Wang, Z.-G. Driving force and pathway in polyelectrolyte complex coacervation. *Proc. Natl. Acad. Sci. U.S.A.* **2022**, *119*, No. e2209975119.

- (138) Adhikari, S.; Prabhu, V. M.; Muthukumar, M. Lower Critical Solution Temperature Behavior in Polyelectrolyte Complex Coacervates. *Macromolecules* **2019**, *52*, 6998–7004.
- (139) Ylitalo, A. S.; Balzer, C.; Zhang, P.; Wang, Z.-G. Electrostatic Correlations and Temperature-Dependent Dielectric Constant Can Model LCST in Polyelectrolyte Complex Coacervation. *Macromolecules* **2021**, *54*, 11326–11337.
- (140) Andersen, H. C.; Chandler, D. Optimized Cluster Expansions for Classical Fluids. I. General Theory and Variational Formulation of the Mean Spherical Model and Hard Sphere Percus-Yevick Equations. *J. Chem. Phys.* **1972**, *57*, 1918–1929.